

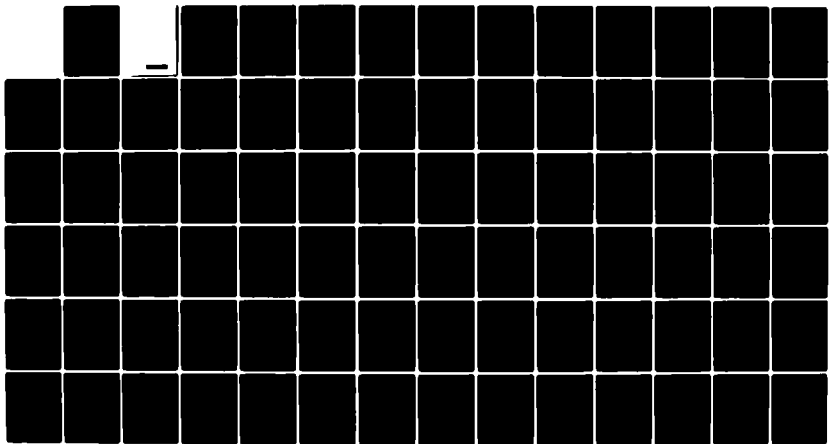
AD-A136 022

INELASTIC DEFORMATION OF METALS AND STRUCTURES UNDER
DYNAMIC AND QUASI-ST. (U) CAIRO UNIV (EGYPT) DEPT OF
MECHANICAL DESIGN AND PRODUCTION.. A M ELEICHE ET AL.
MAY 83 DAJA37-81-C-0236

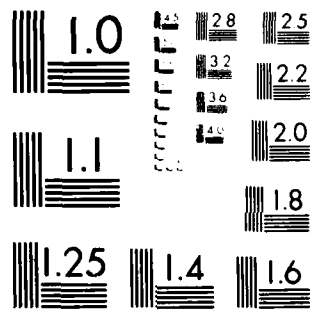
1/1

UNCLASSIFIED

F/G 20/11 NL



END
DATE
FILMED
11 - 84
DTIC



MICROCOPY RESOLUTION TEST CHART
NATIONAL BUREAU OF STANDARDS-1963-A

INELASTIC DEFORMATION OF METALS AND STRUCTURES
UNDER DYNAMIC AND QUASI-STATIC CYCLIC LOADING

Annual Technical Report

A.M. Eleiche and M.M. Megahed

May 1983

United States Army
EUROPEAN RESEARCH OFFICE OF THE U.S. ARMY
London England

CONTRACT NUMBER DAJA37-81-C-0236

Faculty of Engineering
Cairo University

Approved for Public Release; distribution unlimited

UNCLASSIFIED

R&D 2872-AN

SECURITY CLASSIFICATION OF THIS PAGE (When Data Entered)

REPORT DOCUMENTATION PAGE		READ INSTRUCTIONS BEFORE COMPLETING FORM
1. REPORT NUMBER	2. GOVT ACCESSION NO.	3. RECIPIENT'S CATALOG NUMBER
	ADA135 022	
4. TITLE (and Subtitle) Inelastic Deformation of Metals and Structures Under Dynamic and Quasi-Static Cyclic Loading		5. TYPE OF REPORT & PERIOD COVERED Annual Technical Report
		6. PERFORMING ORG. REPORT NUMBER
7. AUTHOR(s) A. M. Eleiche and M. M. Megahed		8. CONTRACT OR GRANT NUMBER(s) DAJA37-81-C-0236
9. PERFORMING ORGANIZATION NAME AND ADDRESS Faculty of Engineering Cairo University		10. PROGRAM ELEMENT, PROJECT, TASK AREA & WORK UNIT NUMBERS 6.11.02A TT161102BH57-06
11. CONTROLLING OFFICE NAME AND ADDRESS USARDSG-UK Box 65, FPO NY 09510		12. REPORT DATE May 83
		13. NUMBER OF PAGES 71
14. MONITORING AGENCY NAME & ADDRESS (if different from Controlling Office)		15. SECURITY CLASS. (of this report) Unclassified
		15a. DECLASSIFICATION/DOWNGRADING SCHEDULE
16. DISTRIBUTION STATEMENT (of this Report) Approved for public release; distribution unlimited		
17. DISTRIBUTION STATEMENT (of the abstract entered in Block 20, if different from Report)		
18. SUPPLEMENTARY NOTES		
19. KEY WORDS (Continue on reverse side if necessary and identify by block number) Cyclic Plasticity, cyclic plastic behaviour, cyclic creep, cyclic hardening, Uniaxial model,		
20. ABSTRACT (Continue on reverse side if necessary and identify by block number) Studies on cyclic plasticity during the second year of the contract has developed along a theoretical approach to the problems involved. It is hoped, however, that this approach will furnish a good basis for useful and meaningful tests on components operating under cyclic plasticity conditions.		

DD FORM 1 JAN 73 1473

EDITION OF 1 NOV 65 IS OBSOLETE

UNCLASSIFIED

SECURITY CLASSIFICATION OF THIS PAGE (When Data Entered)

UNCLASSIFIED

SECURITY CLASSIFICATION OF THIS PAGE(When Data Entered)

The investigations of the modes of cyclic plastic behaviour in tubes under internal pressure and cyclic thermal gradient have been continued. The results obtained so far are summarized in Part 1. An approximate uniaxial model of the biaxial tube problem is used for studying the influence of the hardening rule on the cyclic plastic behaviour. Comparisons are made between kinematic and isotropic hardening rules. These two theories represent the extremes of cyclic plastic behaviour. To avoid the drawbacks of the uniaxial model, a two-dimensional numerical solution utilizing kinematic hardening has been also developed. Results obtained are in better correlation with experiments. Present efforts on the tube problem will make use of a plasticity model which can faithfully represent the observed cyclic hardening and cyclic creep.

In Part 2, the cyclic plastic behaviour of specimens used in the so-called pulley test are studied using linear kinematic hardening theory. The pulley test simulates the cyclic thermal stresses by means of cyclic bending of a thin specimen around the circumference of a freely rotating pulley. Theoretical results for stress and strain behaviour are obtained for both wire and strip specimens. Comparisons with test results show qualitative agreement. In view of these comparisons, greater insight has been gained on the implications of cyclic creep of the behaviour of components operating under cyclic loading.

In Part 3, the reference stress method (RSM) - which has been used with great success in the analysis of creeping structures - is applied to the analysis of components operating under conditions where cyclic hardening and cyclic creep are dominant. The technique is quite simple; it provides a direct relationship between the behaviour of the structure at a given point to the result of a uniaxial test conducted at the reference conditions of stress or strain amplitudes. Accordingly, the analysis is reduced to the determination of the reference test conditions. The elegant procedure obviates the need for extensive testing programmes aimed at describing accurately the behaviour of metal. The technique is illustrated for beams under both uniform and non-uniform bending and comparisons with published test data show excellent agreement.

UNCLASSIFIED

SECURITY CLASSIFICATION OF THIS PAGE(When Data Entered)

FOREWORD

This technical report was prepared by the Department of Mechanical Design and Production, Faculty of Engineering, Cairo University, Egypt. The work reported herein was supported, in part, by the European Research Office of the U.S. Army, London, England, under contract number DAJA 37-81-C-0236.

This report covers work conducted from May 23, 1982 to May 28, 1983. Material behaviour aspects under impact cyclic loading for copper and mild steel are not included in the present report, since testing and analysis of results are still under completion. A full account of that area will be given in the final report.

Most of the work presented herein has been submitted by Dr. Megahed for publication in the open literature, particularly Parts 2 and 3.

The authors are grateful to Mr. A.F. Bastawros, graduate student at Cairo University, for his assistance in the numerical computations and in the preparation of this report.



AI

INELASTIC DEFORMATION OF METALS AND STRUCTURES
UNDER DYNAMIC AND QUASI-STATIC CYCLIC LOADING

by

A.M. Eleiche and M.M. Megahed

ABSTRACT

Studies on cyclic plasticity during the second year of the contract has developed along a theoretical approach to the problems involved. It is hoped, however, that this approach will furnish a good basis for useful and meaningful tests on components operating under cyclic plasticity conditions.

The investigations of the modes of cyclic plastic behaviour in tubes under internal pressure and cyclic thermal gradient have been continued. The results obtained so far are summarized in Part 1. An approximate uniaxial model of the biaxial tube problem is used for studying the influence of the hardening rule on the cyclic plastic behaviour. Comparisons are made between kinematic and isotropic hardening rules. These two theories represent the extremes of cyclic plastic behaviour. To avoid the drawbacks of the uniaxial model, a two-dimensional numerical solution utilizing kinematic hardening has been also developed. Results obtained are in better correlation with experiments. Present efforts on the tube problem will make use of a plasticity model which can faithfully represent the observed cyclic hardening and cyclic creep.

In Part 2, the cyclic plastic behaviour of specimens used in the so-called pulley test are studied using linear kinematic hardening theory. The pulley test simulates the cyclic thermal stresses by means of cyclic bending of a thin specimen around the circumference of a freely rotating pulley. Theoretical results for stress and strain behaviour are obtained for both wire and strip specimens. Comparisons with test results show qualitative agreement. In view of these comparisons, greater insight has been gained on the implications of cyclic creep of the behaviour of components operating under cyclic loading.

In Part 3, the reference stress method (RSM) - which has been used with great success in the analysis of creeping structures - is applied to the analysis of components operating under conditions where cyclic hardening and cyclic creep are dominant. The technique is quite simple; it provides a direct relationship between the behaviour of the structure at a given point to the

result of a uniaxial test conducted at the reference conditions of stress or strain amplitudes. Accordingly, the analysis is reduced to the determination of the reference test conditions. This elegant procedure obviates the need for extensive testing programmes aimed at describing accurately the behaviour of metals. The technique is illustrated for beams under both uniform and non-uniform bending and comparisons with published test data show excellent agreement.

TABLE OF CONTENTS

	Page
<u>Part 1 - Analytical and Numerical Investigations of Thin Tubes Under Internal Pressure and Cyclic Radial Temperature Gradient</u>	1
Abstract	1
1. Introduction	2
2. The Elasto-Plastic Problem	5
3. Elastic Shakedown, Cyclic Plasticity and Ratchetting	8
4. Discussion of Results	11
5. Analysis of Inelastic Benchmark Ratchetting Tests	14
6. Conclusions	18
7. References	19
<u>Part 2 - Kinematic Hardening Analysis of Ratchet Strain in the "Pulley Test"</u>	33
Abstract	33
1. Introduction	33
2. The Equivalent Bree Problem	35
3. Modes of Cyclic Plastic Behaviour	36
4. Accumulation of Ratchet Strain	
a. Kinematic hardening solution	40
b. Perfect plasticity solution	42
5. Discussion of Results and Conclusions	42
6. References	45
<u>Part 3 - Applications of Reference Stress Method (RSM) in Cyclic Plasticity Analysis</u>	55
Abstract	55
1. Reference Stress Method in Creep Analysis	55
2. Cyclic Plasticity Analysis	58

TABLE OF CONTENTS (Cont.)

3. Comparison with Test Results	40
4. Cyclic Creep Analysis	62
5. Conclusions	65
6. References	66

LIST OF ILLUSTRATIONS

Figure		Page
<u>Part 1 - Analytical and Numerical Investigations of Thin Tubes Under Internal Pressure and Cyclic Radial Temperature Gradient</u>		
1a	Transient temperature distribution across the tube wall and its bilinear representation	21
1b	Equivalent uniaxial model, temperature distribution and elastic thermal stress	21
2	Linear kinematic hardening model	21
3	Stresses during the first half cycle	21
4	Modes of behaviour for a uniaxial tube model ($K = 40$, $h = 0.2$)	22
5	Cyclic plasticity and ratchetting behaviour	23
6a	Examples of ratchet strain accumulation ($K = 40$, $h = 0.2$, $\sigma_y/E = 0.18$)	24
6b	Kinematic hardening results for 304 SS at $\sigma_p = 0.675 \sigma_y$ and $\sigma_t = 2.74 \sigma_y$	25
6c	Isotropic hardening results for 304 SS at $\sigma_p = 0.675 \sigma_y$ and $\sigma_t = 2.74 \sigma_y$	26
7	Full solution map and contours of total ratchet strain for a tube with $D/t = 21.51$, $h = 0.328$ using monotonic properties of 304 SS at 900°F ($\sigma_y = 11.15 \times 10^3$ psi, $E = 23.3 \times 10^6$ psi, $\alpha = 11 \times 10^{-6}/^\circ\text{F}$, $K = 38.56$ and $\nu = 0.3$)	27
8a	Stress distributions during first cycle as obtained numerically for $h = 0$ and $h = 0.328$ for both kinematic and isotropic hardening rules, for $\sigma_p = 0.675 \sigma_y$ and $\sigma_t = 2.74 \sigma_y$ for 304 SS	28
8b	Effect of h on ratchet boundary	29
8c	Effect of h on ratchet strain and amplitudes of cyclic plasticity	29
9	Comparison between model predictions and experimental results for test-1	30
10	Characterization of cyclic hardening in 304 SS	31

Figure	Page
<u>Part 2 - Kinematic Hardening Analysis of Ratchet Strain in the "Pulley Test"</u>	
1a	Schematic illustration of the pulley test 47
1b	Samples of observed ratchet strain 47
2	a) Elastic stress field b) Equivalent multi-bar assembly c) Geometry of wire specimen d) Geometry of strip specimen 48
3	The two possible stress fields due to first cooling 48
4	Bree diagrams and contours of ratchet strains 49
5	Transient and steady state stress fields and plastic strains for the ratchetting regimes 50
6	Algorithm for determination of ratchet strain 51
7	Perfect plasticity and kinematic hardening solutions for the accumulation of ratchet strain in a wire specimen 52
8	Comparison between exact perfect plasticity solutions for ratchet strain per cycle and linearized lower bound estimates 53
9a	Operating conditions and Bree diagram for ratchetting tests on copper wires 54
9b	Applicability of Eq. (18) for estimation of primary ratchet strains in the copper wire tests 54
<u>Part 3 - Applications of Reference Stress Method (RSM) in Cyclic Plasticity Analysis</u>	
1	Monotonic, ith cycle and steady state cyclic stress-strain curves for 99.9% pure copper 68
2a	Monotonic stress-strain curve for pure copper 69
2b	Test data and reference stress predictions for a 4-point beam bending test on pure copper 69

3	Cyclic steady-state behaviour for	
	a) beam under cyclic curvature	
	b) solid bar under cyclic twist	70
4a	RSM predictions of test results of simple beam under cyclic central deflection	71
4b	RSM predictions of test results of simple beam under cyclic central load	71

PART 1

ANALYTICAL AND NUMERICAL INVESTIGATIONS OF THIN TUBES UNDER INTERNAL PRESSURE AND CYCLIC RADIAL TEMPERATURE GRADIENT

Abstract

The elasto-plastic behaviour of thin tubes under internal pressure and cyclic radial thermal gradient is investigated for non-linear temperature distribution across the tube wall. The following simplifying assumptions are introduced: 1) an equivalent uniaxial model, which ignores the effect of axial stress on the tube behaviour, is adopted, 2) the non-linear temperature distribution is approximated by means of a bilinear relation, 3) the plastic behaviour of the material is represented by a linear kinematic hardening model. The numerical procedure is modified to handle the isotropic hardening rule in a similar manner to that for handling kinematic hardening.

Results of this investigation show that the bilinear temperature distribution introduces new modes of cyclic plastic deformation which are not present for linear distribution. Also, the bilinear distribution is found to cause more stringent ratchetting limits, larger ratchet strains and larger amplitudes of cyclic plasticity when compared with those due to the linear distribution.

The numerical programme is further improved so as to solve the tube problem in a generalized plane strain form, i.e. in two dimensions, and thus the need for an equivalent uniaxial model no longer exists. This two dimensional numerical solution is

also modified to include isotropic hardening. Outputs of the programme for the uniaxial model under both kinematic and isotropic hardening rules as well as those for the biaxial model under the kinematic hardening rule are in good agreement with analytical and experimental results. The biaxial model under the isotropic hardening rule is still under convergence and accuracy checks.

The results are also compared with experimental results available in the literature for the plastic ratchetting of thin tubes tested in a sodium loop and operating above the shakedown limit.

1. Introduction

A unique high temperature structural design problem in the Liquid-Metal-Fast-Breeder-Reactor (LMFBR) results from the frequent thermal transients that can occur in heat exchanger tubes during the reactor startups and shutdowns. These intermittent thermal shocks can produce progressive inelastic deformation (ratchetting) and significant fatigue damage.

Ratchetting of pressurized thin tubes under cyclic thermal transients has been investigated by Miller /1/ and Bree /2/ using perfect plasticity assumptions. Mulcahy /3/ realized the unrealistic representation of the behaviour of austenitic steels by perfect plasticity and therefore analysed the tube

problem using a linear kinematic hardening model. These studies consider a linear temperature distribution across the tube wall. In practice, however, temperature is distributed non-linearly across the wall as seen in Fig. 1a which reproduces the basic features of Corum et al /4/ tests on ratchetting of 304 stainless steel tubes. Although the kinematic hardening model accounts for an idealized Bauschinger effect, it does not reproduce some equally important facts of the cyclic plastic behaviour of metals such as cyclic hardening, cyclic creep (material ratchetting) and cyclic relaxation.

In the present work, the non-linear temperature distribution across the tube wall is taken into account by means of a bilinear approximation. A linear kinematic hardening model is used for the analysis and both the kinematic and isotropic hardening models are employed in the numerical solution. In common with previous work, /1/, /2/ and /3/, the two-dimensional tube problem is reduced to an equivalent uniaxial one by ignoring the effects of the axial membrane stress and magnifying the thermo-elastic stress.

The elasto-plastic solution is obtained in a semi-analytical form and the computer is employed to perform some of the tedious manipulations associated with the ratchetting regimes. The results show that the bilinear temperature distribution introduces new modes of deformation not associated with the linear distribution /1,2,3/. For example, operating conditions

above shakedown will exhibit cyclic plasticity which is confined to the inner skin of the tube only as compared with cyclic plasticity at both the inner and outer skins for the linear temperature distribution. Also, the bilinear distribution introduces more stringent ratchetting limits, larger ratchet strains and larger amplitudes of cyclic plasticity at the inner skin of the tube wall, which in turn enhances fatigue damage in the tube /5/. The previous arguments are found to be true for isotropic hardening as could be seen from the numerical results.

The two-dimensional kinematic hardening solution technique gave similar regimes of deformation to those obtained from the uni-axial model. Although the stress distribution at a certain cycle is not very much different in magnitudes, its form is considerably different from those obtained for the uniaxial model. This may be attributed to the bi-axiality effects. Also the ratchet strains, cumulative strains and amplitudes of cyclic plasticity are markedly lower than those for the equivalent uniaxial model.

The present elasto-plastic results are used to analyse the tube ratchetting tests carried out by Corum et al /4/ on thin tubes made from initially annealed 304 stainless steel under severe thermal downshocks between 1100°F and 800°F , Fig. 1a. In these tests, each thermal shock is followed by a hold period at 1100°F which causes accumulation of time-dependent

creep strains. This creep strains can be evaluated using the technique developed by Ainsworth /6.7/ which yields an upper bound on creep deformation per cycle when load variations exceed the shakedown limit.

2. The Elasto-Plastic Problem

Consider a thin tube (inner radius a and outer radius b) under an internal pressure P and a cyclic thermal gradient of maximum value ΔT distributed non-linearly across its wall thickness t. The non-linear temperature distribution may be approximated by means of a bilinear relation such that :

$$T(x) = 0 \quad \text{for } 0 \leq x \leq h$$

$$T(x) = - \Delta T (x-h)/(1-h) \quad \text{for } h \leq x \leq 1$$

where $x = (b-r)/t$, i.e. $x = 0$ at $r = b$ and $x = 1$ at $r = a$

Elastic thermal stresses are given by (/8/):

$$\begin{aligned} \sigma_{\theta} = \sigma_z &= - (1-h) \frac{E\alpha \Delta T}{2(1-\nu)} \quad \text{for } 0 \leq x \leq h \\ \sigma_{\theta} = \sigma_z &= - (1-h) \frac{E\alpha \Delta T}{2(1-\nu)} + \frac{x-h}{1-h} \frac{E\alpha \Delta T}{1-\nu} \quad \text{for } h \leq x \leq 1 \end{aligned} \quad (2)$$

These stresses are cyclically superimposed upon the membrane stresses due to internal pressure, which are given by

$$\sigma_{\theta} = 2\sigma_z = \frac{PD}{2t} \quad (4)$$

where D is the mean diameter of the tube.

As argued by Bree /2/, the effect of σ_z is opposite that of σ_{θ} , and hence ignoring σ_z should yield conservative

strain estimates. This reduces the two dimensional problem to that of a slab prevented from bending and subjected to a steady mechanical stress $\sigma_p = PD/2t$ in addition to the temperature cycle given by equations (1), Fig. 1b. The corresponding uniaxial thermal stresses are,

$$\begin{aligned}\sigma_t(x) &= - (1-h)\sigma_t && \text{for } 0 \leq x \leq h \\ \sigma_t(x) &= - (1-h)\sigma_t + 2 \frac{(x-h)}{(1-h)} \sigma_t && h \leq x \leq 1\end{aligned}\tag{5}$$

where $\sigma_t = \frac{1}{2} E\alpha\Delta T/(1-\nu)$ is one half of the total thermal stress across the tube wall, Fig. 1b. An operating condition will therefore be defined in terms of σ_p and σ_t .

The elasto-plastic analysis is carried out using a linear kinematic hardening material model, Fig. 2, where the slope of the plastic portion is assumed to be a constant βE . This yields the flow rule as,

$$d\epsilon_p = \frac{1-\beta}{\beta E} d\sigma = \frac{K}{E} d\sigma\tag{6}$$

where $K = (1-\beta)/\beta$ is the material hardening parameter. For simplicity, all material constants E , ν , α , K and σ_y are assumed to be temperature independent.

In the isothermal condition, the uniaxial model is subjected to a uniform stress σ_p , and upon application of the thermal gradient during the first half cycle, the stresses will increase in the cold fibers and decrease in the hot ones.

Consequently, two distinct stress fields are possible, the first involves tensile yielding only, Fig. 3a, and the second involves both tensile and compressive yielding, Fig. 3b. The elasto-plastic stress-strain relations for the stress field of Fig. 3a are:

$$\begin{aligned} \epsilon_1 &= \sigma_1(x)/E && \text{for } 0 < x < h \\ \epsilon_1 &= [\sigma_1(x) - 2\sigma_t(x-h)/(1-h)]/E && \text{for } h < x < y_1 \quad (7) \\ \epsilon_1 &= [\sigma_1(x) - 2\sigma_t(x-h)/(1-h) + K(\sigma_1(x) - \sigma_y)] && \text{for } y_1 < x < l \end{aligned}$$

where y_1 is the plastic front. Equilibrium and compatibility conditions are expressed by:

$$\sigma_p = \int_0^l \sigma_1(x) dx \quad \text{and} \quad \epsilon_1 = \text{constant} \quad (8)$$

Since $\sigma_1(y_1) = \sigma_y$, the constant ϵ_1 becomes equal to $[\sigma_y - 2\sigma_t(y_1-h)/(1-h)]/E$ and the integrals in the equilibrium equation can now be evaluated to yield y_1 as:

$$y_1 = -\frac{1}{K} + \frac{1}{K} \sqrt{(1+K)(1+Kh^2) + K(1+K)(1-h)(1-\sigma_p/\sigma_y) \cdot \sigma_y/\sigma_t} \quad (9)$$

Fully elastic behaviour is assured if $y_1 > l$ which implies (using Eq. (9)) that:

$$\sigma_t < (\sigma_y - \sigma_p)/(1+h) \quad (10)$$

Compressive yielding occurs at $x = 0$ if $\sigma_1(0) < -\sigma_y$ which is equivalent to (using Eq. (9)):

$$(\sigma_t/\sigma_y)^2 + [(1+K)(1-\sigma_p/\sigma_y) - 2(1+Kh)]. (\sigma_t/\sigma_y)/(1-h) - K > 0 \quad (11)$$

Operating conditions which satisfy inequality (11) will cause both tensile and compressive yielding during the first half cycle (Fig. 3b) and the solution of the corresponding elasto-plastic problem yields the following expression for the strain ϵ_1 :

$$\epsilon_1 = [\sigma_y - 2\sigma_t(y_1 - h)/(1-h)]/E = -[\sigma_y + 2\sigma_t(z_1 - h)/(1-h)]/E, \text{ where}$$

$$y_1 = \frac{(1+h^2)(\sigma_t/\sigma_y)^2 + (1-h)(1+K)(1-\sigma_p/\sigma_y) \cdot \sigma_t/\sigma_y + K(1-h^2)}{2 \cdot \sigma_t/\sigma_y (\sigma_t/\sigma_y + K(1-h))} \quad (12)$$

Subsequent thermal cycling gives rise to either elastic shakedown, cyclic plasticity or ratchetting, as shown in Fig. (4).

3. Elastic Shakedown, Cyclic Plasticity and Ratchetting

For operating conditions which satisfy Eq. (11), the stress fields shown in Figs. 5a and 5b are possible during the second half cycle. The stress field of Fig. 5a involves cyclic plasticity at the inner skin of the tube while the stress field of Fig. 5b involves cyclic plasticity at both the inner and outer skin of the tube.

The elasto-plastic analysis of the stress field in Fig. 5a yields the plastic front y_2 given by Eq. (13)

$$y_2 = -\frac{1}{K} + \frac{1}{K} \sqrt{(1+K)(1+Kh^2) + 2K(1+K)(1-h)\sigma_y/\sigma_t} \quad (13)$$

Shakedown will occur if $y_2 \geq 1$ which is satisfied if

$$\sigma_t \leq 2\sigma_y/(1+h) \quad (14)$$

and such shakedown behaviour is termed as S_1 (Fig. 4). In Fig. 5a, cyclic plasticity will not occur at the outer skin ($x=0$) if $\Delta\sigma_2(0) < 2\sigma_y$ and such condition is satisfied if

$$\sigma_t \leq \sigma_y \left[\frac{\sqrt{(K-2Kh-1)^2 + 4K(1-h)^2} - (K - 2Kh-1)}{(1-h)} \right] \quad (15)$$

Thus, thermal stresses which satisfy Eq. (15) but violate Eq. (14) produce cyclic plasticity at the inner skin only, and such behaviour is called F_1 in Fig. 4. Note that for $h = 0$, Eqs. (14) and (15) become identical, viz. $\sigma_r \leq 2\sigma_y$ and regime F_1 is not present as in Mulcahy's analysis /3/ for linear temperature distribution.

The stress field of Fig. 5b will occur when thermal stresses violate Eq. (15) and cyclic plasticity takes place at both the inner and outer skin of the tube. Such behaviour is termed F_2 in Fig. 4. It can be shown that F_2 will continue during subsequent temperature cycling if

$$\left[(1+Kh^2) - (1+K)\sigma_p/\sigma_y \right] \cdot (\sigma_t/\sigma_y)^2 + K(1-h) \left[3 - 2(1+K)\sigma_p/\sigma_y \right] \cdot \sigma_t/\sigma_y + 2K^2 (1-h)^2 > 0 \quad (16)$$

as shown in Fig. 4.

Cyclic plasticity may also take place when the response of the model exhibits tensile yielding only during the first half cycle (Fig. 3a). A possible second half cycle stress field which corresponds to such behaviour is shown in Fig. 5c and the corresponding plastic front y_2 is given by Eq. 17.

$$y_2 = -\frac{1}{K} + \frac{1}{K} \sqrt{(1+K)(1+Kh^2) + 2K(K+1)(1-h) \cdot \sigma_y/\sigma_t} \quad (17)$$

This mode of cyclic plasticity is similar to the reversed plasticity is confined to the inner skin only. Such behaviour is termed F_3 in Fig. 4 and it can be shown that the condition for its continuation during subsequent thermal cycling is

$$[(1+K)(1+\sigma_p/\sigma_y)^2 - 4(1+Kh^2)] \cdot (\sigma_t/\sigma_y)^2 - 2K(1-h)(3-\sigma_p/\sigma_y) \cdot \sigma_t/\sigma_y + K^2(1-h^2)/(1+K) < 0 \quad (18)$$

Shakedown will occur if $y_2 \geq 1$ and $\sigma_2(0) < \sigma_y$ and these conditions are satisfied if,

$$\sigma_t < \frac{4(1+K)}{K(1+h)(1-h^2)} (\sigma_y - \sigma_p) \quad \text{and} \quad \sigma_t < 2\sigma_y/(1+h) \quad (19)$$

This shakedown behaviour is termed S_2 in Fig. 4.

Ratchetting takes place for operating conditions which violate Eqs. (16), (18) or (19) as can be seen from Fig. 4 for the ratchetting regimes R_1 , R_2 , R_3 and R_4 . In the ratchetting regime R_1 , which takes place at thermal stresses below the shakedown limit ($\sigma_t = 2\sigma_y/(1+h)$), a cyclic stress field which produces cyclic permanent deformation is shown in Fig. 5d.

The accumulated ratchet strain is obtained through numerical evaluation of the recurrence relations for the corresponding y_n and y_{n+1} by a simple computer algorithm. Elastic shakedown is approached asymptotically as the cyclic steady state following an initial phase of transient ratchetting.

In regime R_2 , transient ratchetting takes place while cyclic plasticity is occurring at both the inner and outer skin

of the tube (Fig. 5e) until a cyclic steady state similar to F_2 is approached asymptotically. In regime R_3 , the transient response consists of two consecutive phases of ratchetting mechanisms. In the first phase, ratchetting takes place according to a mechanism similar to that present in R_1 until a sufficient degree of hardening is attained such that the mechanism shown in Fig. 5f is activated. In this second phase of R_3 , ratchetting is developed while cyclic plasticity is taking place at the inner skin of the tube. Clearly, the cyclic steady state for R_3 will be similar to that present in F_1 and F_3 . In the ratchetting regime R_4 , ratchetting is developed through three consecutive phases. R_1 is employed in the first phase, the second phase is similar to the second phase of R_3 and the third phase is the same as R_2 . Consequently, the cyclic steady state for F_2 , R_2 and R_4 are similar.

When a linear temperature distribution ($h=0$) is assumed across the tube wall, the resulting cyclic steady state is either shakedown for $\sigma_t < 2\sigma_y$ or cyclic plasticity at both the inner and outer skin of the tube for $\sigma_t > 2\sigma_y$. It is now clear that due to the bilinear temperature distribution ($h > 0$), new modes of behaviour (F_1 , F_3 and R_3) are discovered in which cyclic plasticity is confined to the inner skin of the tube.

4. Discussion of Results

The results of previous sections were assembled into a computer program described in detail in a previous report /9/ whose input is the problem parameters $1 < K < \infty$, $0 < h < 0.5$

and the operating condition as defined by $0 < \sigma_p < \sigma_y$ and $0 < \sigma_t < \infty$. The program is provided with 10 routines which yield stresses and strains corresponding to $E, S_1, S_2, F_1, F_2, F_3, R_1, R_2, R_3$ and R_4 . In the ratchetting regimes, the cyclic steady state is assumed to be reached when $\Delta \epsilon_p(x=0)$ does not change by more than 10^{-6} per cycle. Examples of the transient ratchetting behaviour in R_1, R_2, R_3 and R_4 are shown in Fig. 6a. It is seen that most of the ratchet strain accumulates during the first 20 cycles or so. The number of cycles required to reach the steady state depends mainly on the hardening parameter K . As K becomes larger, the material plastic behaviour approaches that of perfect plasticity and consequently a larger number of cycles is required before the steady state is reached. However, for austenitic and many high strength steels $K \approx 40 - 50$ which imply that the steady state will be reached after the first 20 to 30 cycles.

In Fig. 6b the effect of h is clear. The ratchet strains as well as the cumulative strain are considerably lower in the case of linear temperature distribution ($h=0$) than for the bilinear distribution. This is true for both kinematic hardening and isotropic hardening results as could be seen from Fig. 6c.

An overall view of the results may be gained from the contours of total ratchet strains as shown in Fig. 7 for a thin tube made from 304SS whose monotonic properties at 900°F are used to calculate pressures, temperatures and strains. It

may be noted that the contours of equal ratchet strains are almost parallel to the ratcheting limit (the line which separates R regions from S and F regions) and, correspondingly, ratchet strains are more sensitive to changes in pressures than changes in temperatures. In fact, ratchet strains are reduced slightly as ΔT becomes very large (for $\Delta T > 250^{\circ}\text{F}$ in Fig. 7). However, these large temperature differences are not likely to be encountered in practice.

The important result which emerges from the present work is the effect of the bilinear temperature distribution parameter h on the tube behaviour. As stated earlier, for $h > 0$ new modes of deformation (F_1 , F_3 and R_3) are introduced in which cyclic plasticity is confined to the inner skin of the tube. This is shown in Fig. 8a where it can be seen how h affects the form of stress distribution for a certain set of loading parameters (those used in Corum's tests). The cyclic plasticity at the inner surface of the tube observed for $h = 0.328$ is not present for $h = 0$. This is true for both kinematic and isotropic hardening solutions.

Figure 8a shows the effect of h on the ratchetting limit and it is seen that ratchetting starts to take place at smaller mechanical loads as h becomes larger. This effect is more prominent above the shakedown limit ($\sigma_t = 2\sigma_y$). Fig. 8c shows the effect of h on asymptotic ratchet strain at $\sigma_p = 0.4\sigma_y$, $\sigma_t = 3\sigma_y$. It is seen that ratchet strain attains a maximum

value at $h \approx 0.27$. Thus, an analysis based on linear temperature distribution is likely to underestimate the likelihood of ratchetting as well as the value of ratchet strain. The effect of h on the amplitudes of cyclic plasticity which are of interest when designing against low cycle fatigue is shown in Fig. 8c. At $h = 0$, cyclic plasticity of equal amplitude takes place at both the inner and outer skin of the tube and as h becomes larger, cyclic plasticity amplitudes increase at the inner skin ($x=1$) and decrease at the outer skin ($x=0$). For example, at $h = 0$, $\Delta\epsilon_p(0) = \Delta\epsilon_p(1) = 1.5\sigma_y/E$ while at $h = 0.3$, $\Delta\epsilon_p(1) = 3\sigma_y/E, \Delta\epsilon_p(0) = 0$ which means that the higher value of h doubles the amplitude of cyclic plasticity at $x = 1$. This can be shown to reduce the fatigue life by about thirty percent (using the Coffin-Manson relation $5/\Delta\epsilon_p \cdot N_f^{0.5} = \text{constant}$).

5. Analysis of Inelastic Benchmark Ratchetting Tests

Two thermal ratchetting tests have been conducted by Corum et al /4/ on 304SS thin tubes. In the first test, a tube was subjected to 13 thermal downshocks between 1100°F and 800°F in a sodium loop under internal pressure of 700 psi which is reduced to zero for 2 hrs subsequent to each thermal shock in order to transfer the liquid sodium from the drain to the source tank. Following each thermal shock, the tube was kept at 1100°F for 160 hr. The measured temperature distribution across the tube wall (Fig. 1a) was non-linear and may be reasonably approximated by a bilinear relation with $h = 0.328$

as discussed earlier. The maximum temperature difference across the wall was about 167°F and corresponds to an outer skin temperature of 1000°F and an inner skin temperature of 830°F.

Using the monotonic properties at an average temperature of 900°F, the full solution map is constructed as shown previously in Fig. 7 which shows that the operating conditions of this test lie within the ratchetting regime R_3 . The cyclic accumulation of ratchet strain calculated on the basis of monotonic data at 900°F is shown in Fig. 9 as dotted lines.

Ainsworth /6,7/ developed a method by which an upper bound on creep strain per cycle can be determined for structures subjected to load variations above the shakedown limit. The creep strain is bounded by the cyclic plasticity solution of a similar structure that does not creep. Thus, considering a uniaxial tube model subjected to internal pressure $P(t)$ and cyclic temperature $T(x,t)$, both of cycle τ , and denoting the cyclic plasticity solution for a similar structure, which does not creep, subjected to the loading conditions $P(t) + \rho$ and $T(x,t)$ by $\sigma^*(x,t)$, an upper bound for axial creep displacement is given by

$$\Delta u < \frac{1}{n\rho} \int_0^\tau \int_V \dot{D} \left[\frac{n}{n+1} \sigma^*(x,t) \right] dV dt, \quad (20)$$

where ρ is an additional constant positive load yet to be determined and \dot{D} is the rate of creep energy dissipation.

The bound is evaluated at the value of ρ which minimizes the right-hand side of Eq. (20). Note that the earlier analysis of the elasto-plastic problem yields the stress field $\sigma^*(x,t)$. Assuming that creep is governed by Norton's law and substituting for \dot{D} by $K\sigma^n$, Eq. (20) becomes,

$$\Delta u \leq K \frac{\tau}{n} \left(\frac{n}{n+1}\right)^{n+1} \frac{1}{\rho} \int_0^l \sigma^*(x)^{n+1} dx, \quad (21)$$

Most of the creep strain takes place at the hold temperature of 1100°F and the short term creep rates /10/ at 1000-2000 hrs are used for evaluation of the bound for the test. The stress index n is obtained as $n = 3.655$, /10/, at the level of stresses present in the tests.

The final predictions of plastic and creep ratchetting are compared with experimental results of the test in Fig. 9. The values of yield stress are $\sigma_y = 11.15$ ksi during the first half cycle and $\sigma_y = 14.47$ ksi during subsequent cycling which corresponds to a cyclic plasticity amplitude of $\pm 0.05\%$ as obtained from initial calculations based on the monotonic data at 900°F. The creep strain is 0.0156% per cycle which corresponds to an optimum additional pressure $\rho = 346.4$ psi. Fig. 9 shows that the theoretical predictions are in excess of the observed strains by about 40% for the test.

The predicted ratchet strains are found to be very large when compared with the experimentally observed ratchet strains (the experimental results for the test are also shown

in Fig. 9). This overestimation of observed strains is seen to be due to the use of the monotonic stress - strain data and the kinematic hardening rule which ignore the cyclic hardening properties of the tube material.

The cyclic hardening behaviour of 304SS is characterized in Fig. 10 which shows the percent increase in yield stress against the number of cycles and the amplitude of reversed plastic strain. Yield stress is defined here on the basis of bilinear representation of cyclic hardening loops /10/. The method suggested here to account for cyclic hardening makes use of the monotonic yield stress during the first half cycle only and the 13th cycle yield stress for subsequent cycling. The 13th cycle yield stress is evaluated at an amplitude of cyclic plasticity $\Delta\epsilon_p$ which is representative of the test conditions. An upper bound for $\Delta\epsilon_p$ can be evaluated on the basis of the monotonic data. This approach, however, ignores the effects of other important phenomena such as cyclic creep (material ratchetting) and cyclic relaxation, which are present when plastic cycling takes place around a mean value of stress and strain respectively.

One obvious reason behind the conservatism of the predictions is the modelling of the biaxial tube problem by means of an equivalent uniaxial model in which the equivalence is based on the stresses given in Fig. 9. The uniaxial model

is likely to predict larger hoop strain accumulation. The results of the biaxial kinematic hardening programme are also shown in Fig. 9. These seem to be the nearest to the experimental results though creep strains are not taken into consideration. This may be attributed to the lack of interaction between plasticity and creep in the classical theories of inelastic deformations used in the present analysis.

It is also possible that creep strains are reduced due to prior cyclic hardening /11/. However, in the absence of reliable constitutive relations which accounts for this interaction, classical theories provide conservative strain estimates for the conditions of the present tests.

6. Conclusions

The main conclusions of the present work can be summarized as follows :

1. Comparisons between the modes of behaviour for linear and bilinear temperature distributions across the tube wall show that a bilinear distribution introduces new modes of deformation in which cyclic plasticity is confined to the inner skin of the tube.
2. Also, bilinear distributions are shown to introduce more stringent ratchetting limits above the shakedown limit, larger ratchet strains and larger cyclic plasticity amplitudes at the inner skin of the tube when compared with corresponding linear distribution.

3. It is demonstrated that the cyclic hardening phenomenon should be taken into account in the analysis of ratchetting components above the shakedown limit. An approximate method which accounts for cyclic hardening is used in the present work.
4. The equivalent uniaxial model of thin tubes yields conservative estimates of observed strains in tube ratchetting tests and the biaxial model was found to be very close to the experimental results, though cyclic creep and relaxation are ignored.
5. The inclusion of the isotropic hardening rule into the computer programme increased the ratchet strains and changed the solution map completely. This is to be further investigated in future work.

7. References

1. Miller, P.R., "Thermal Stress Ratchet Mechanisms in Pressure Vessels", J. Basic Engineering, Trans. ASME, Series D, 81, 190-196 (1959).
2. Bree, J., "Elasto-Plastic Behaviour of Thin Tubes Subjected to Internal Pressure and Intermittent High-Heat Fluxes with Application to Fast-Nuclear Reactors Fuel Cans", J. Strain Analysis, 2, 226-238 (1967).
3. Mulcahy, T.M., "Thermal Ratchetting of a Beam Element Having an Idealized Bauschinger Effect," Trans. ASME, J. Engineering Mat. and Tech., 264-271 (1976).

4. Corum, J.M. et al., "Thermal Ratchetting in Pipes Subjected to Intermittent Thermal Downshocks at Elevated Temperatures", 2nd Int. Congress on Pressure Vessels and Piping, San Fransisco, CA, U.S.A. (1975).
5. Coffin, L.F., "Fatigue at High Temperature-Predictions and Interpretation", James Clayton Lecture, Proc. Inst. Mech. Engrs. 188, 109-127 (1974).
6. Ainsworth, R.A., "Bounding Solutions for Creeping Structures Subjected to Load Variations Above the Shakedown Limit", Int. J. Solids and Structures, 13, 971-980 (1977).
7. Ainsworth, R.A., "Applications of Bounds for Creeping Structures Subjected to Load Variations Above the Shakedown Limit", Int. J. Solids and Structures, 13, 981-993 (1977).
8. Timoshenko, S. and Goodier, J.N., "Theory of Elasticity", 3rd Edition, McGraw-Hill Book Co., New York (1970).
9. Eleiche, A.M. and Megahed, M.M. "Inelastic Deformation of Metals and Structures Under Dynamic and Quasi-static Cyclic Loading", Annual Tech. Rept. to ERO, Contract Number DAJA37-81-C-0236, May 1982.
10. Leckie, F.A., Hayhurst, D.R. Megahed, M.M. and Ranaweera, M.P., "Analysis of Inelastic Benchmark Problems", Report to UKAEA Under Agreement No. 4R 53146B, Section 6, (1979).
11. "Mechanical Properties Test Data for Structural Materials", Quarterly Progress Report, ORNL, U.S.A. (1974).

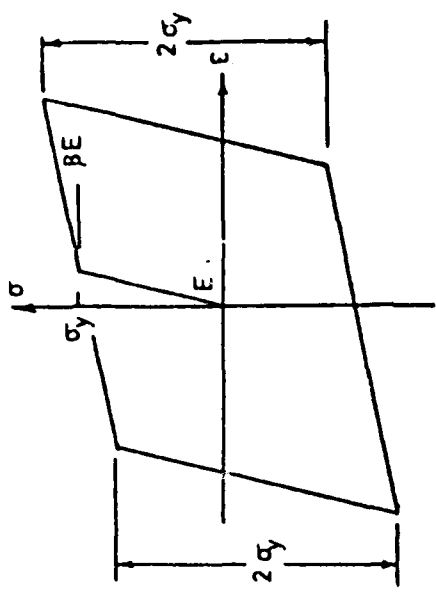
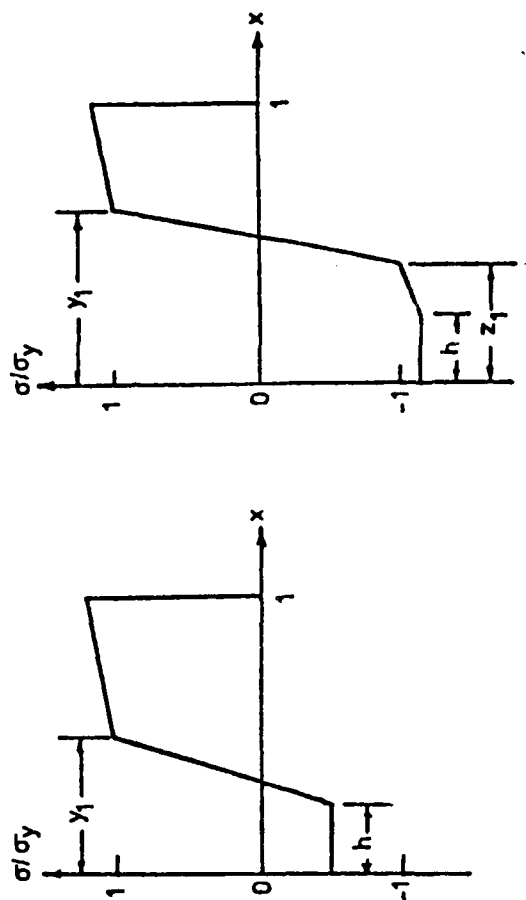


Fig 2 Linear kinematic hardening model



a) Tensile yielding only b) Tensile and compressive yielding
 Fig 3 Stresses during the first half cycle

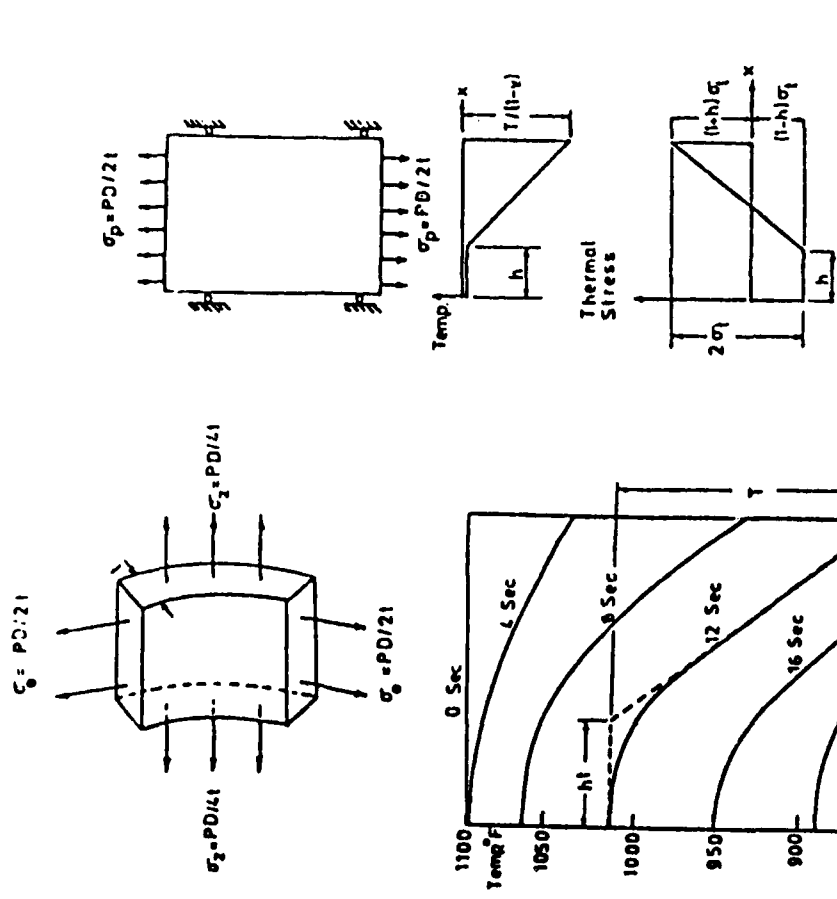


Fig 1b Equivalent uniaxial model, temperature distribution and elastic thermal stress

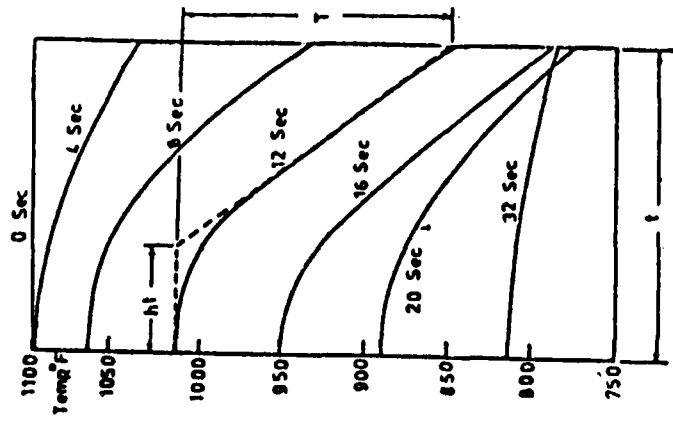


Fig 1a. Transient temperature distribution across the tube wall (c) and its bilinear representation

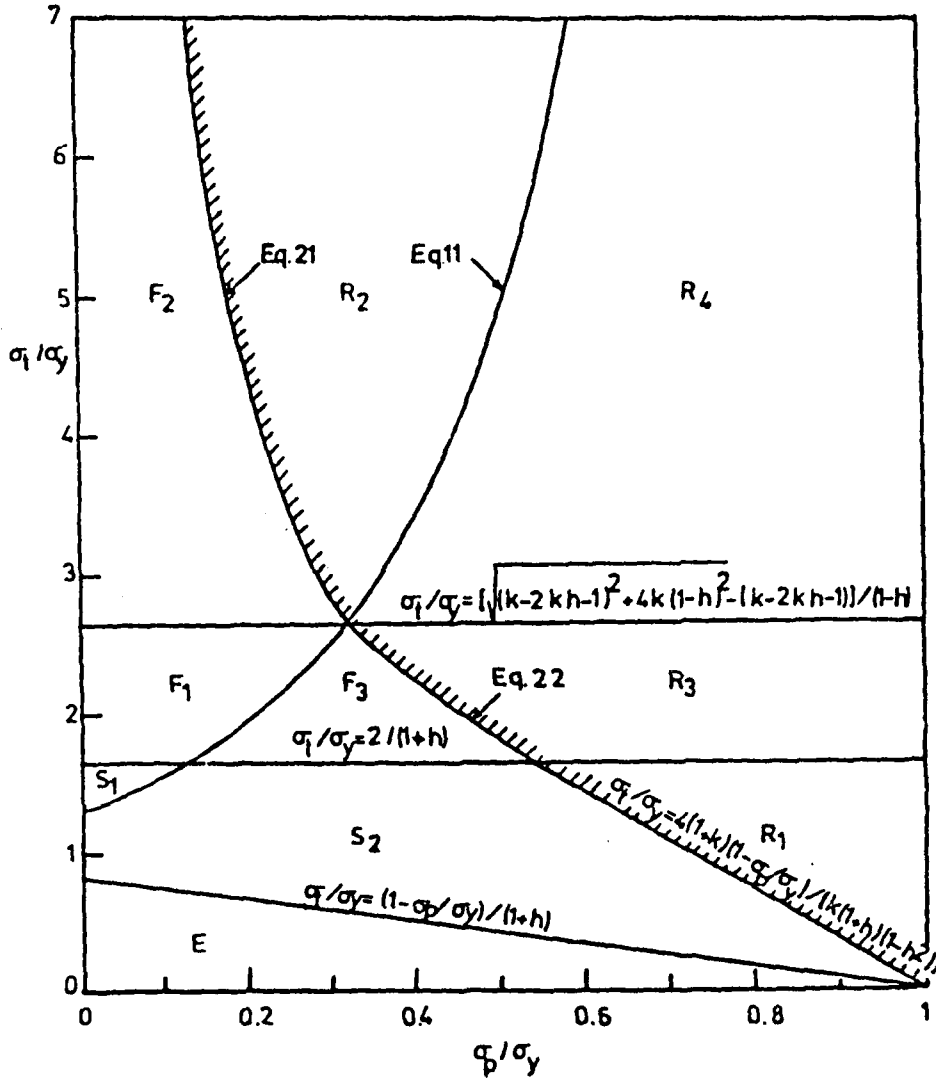


Fig 4 Modes of behaviour for a uniaxial tube model ($K=40, h=0.2$)

- E Fully elastic behaviour
- S₁, S₂ Elastic shakedown
- F₁, F₂, F₃ Cyclic plasticity
- R₁, R₂, R₃, R₄ Ratchetting

CYCLIC PLASTICITY

RATCHETTING

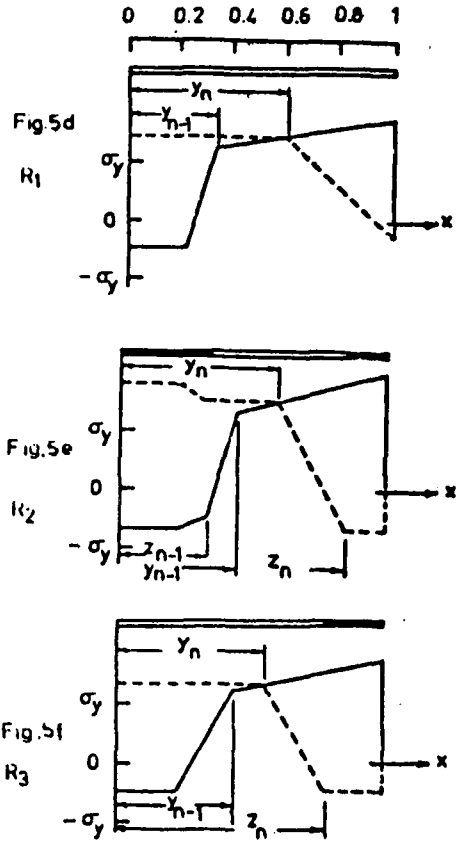
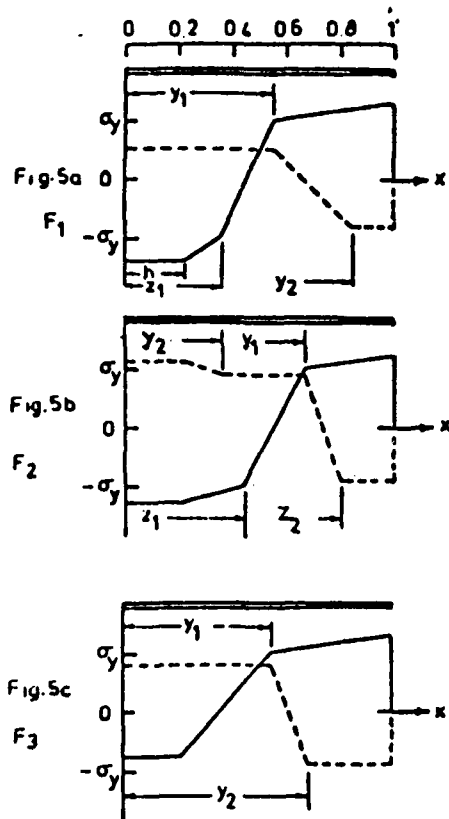


Fig. 5 Cyclic plasticity and ratchetting behaviour
 fibers under cyclic plasticity
 n even number of half cycles

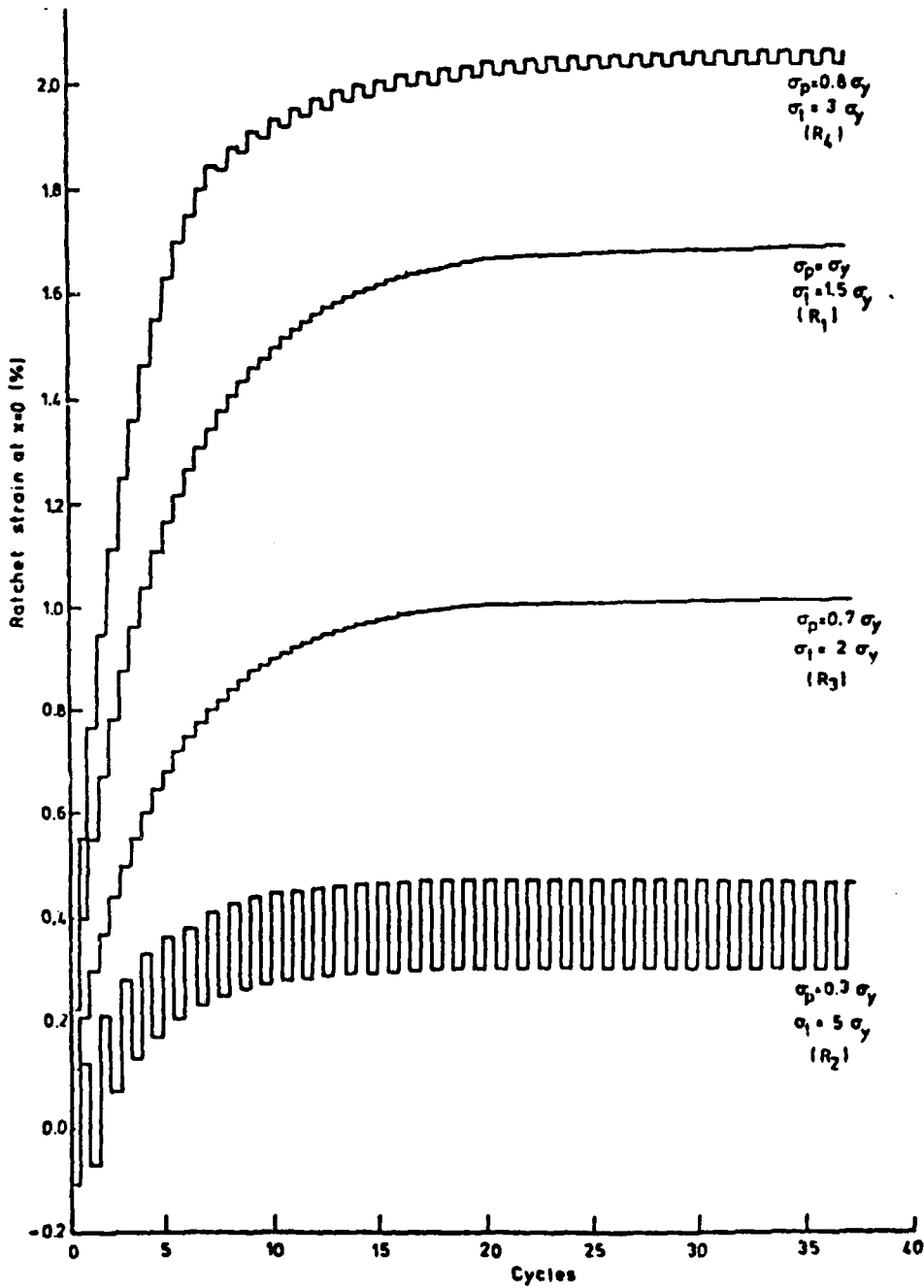


Fig. 6. Examples of ratchet strain accumulation ($K=40, h=0.2, \sigma_y/E=0.1\%$)

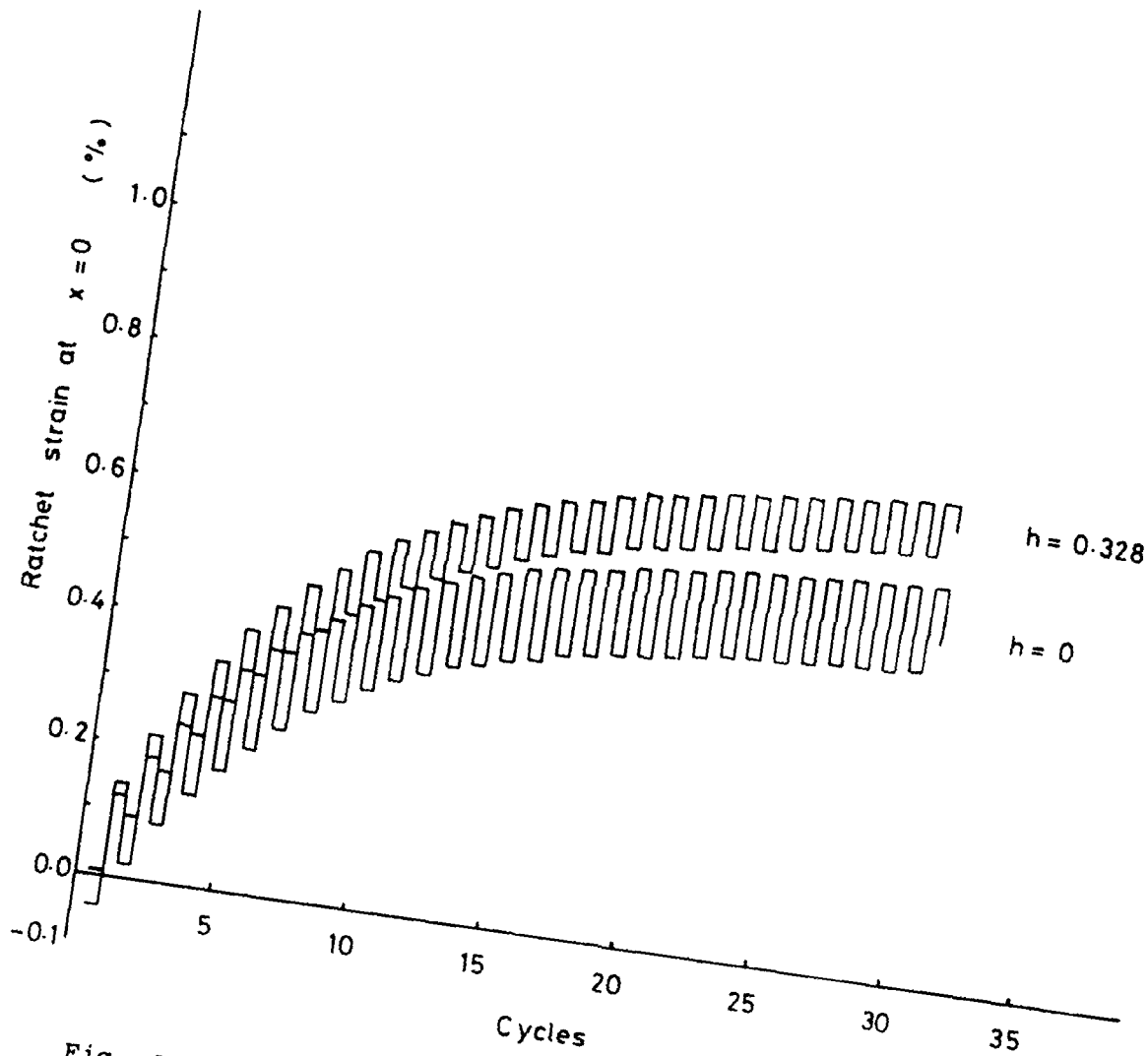


Fig. 6b Kinematic hardening results for 304 SS at $\sigma_p = 0.675 \sigma_y$
and $c_t = 2.74 \sigma_y$

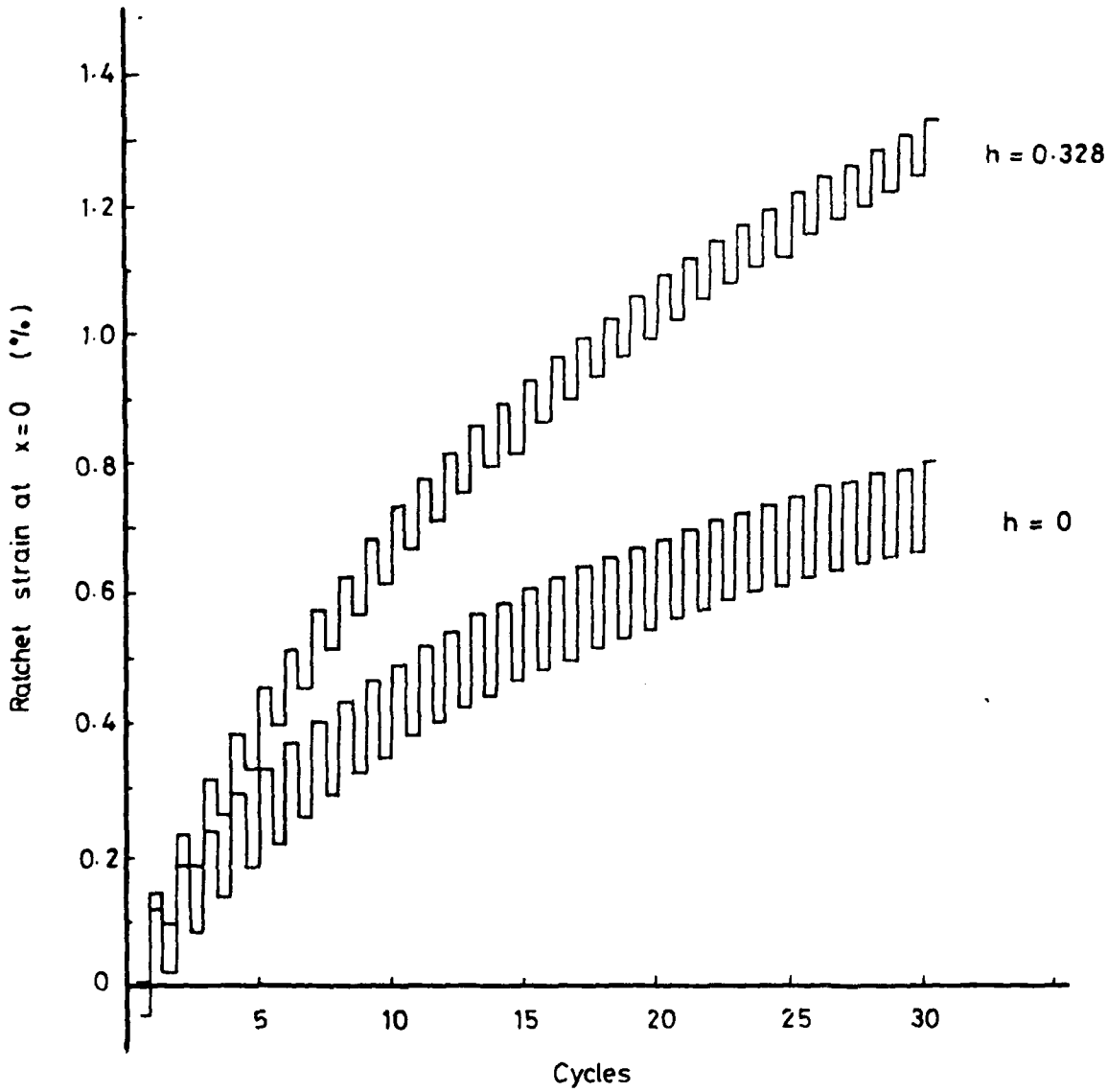


Fig. 6c Isotropic hardening results for 304 SS at $\sigma_p = 0.675 \sigma_y$ and $\sigma_t = 2.74 \sigma_y$

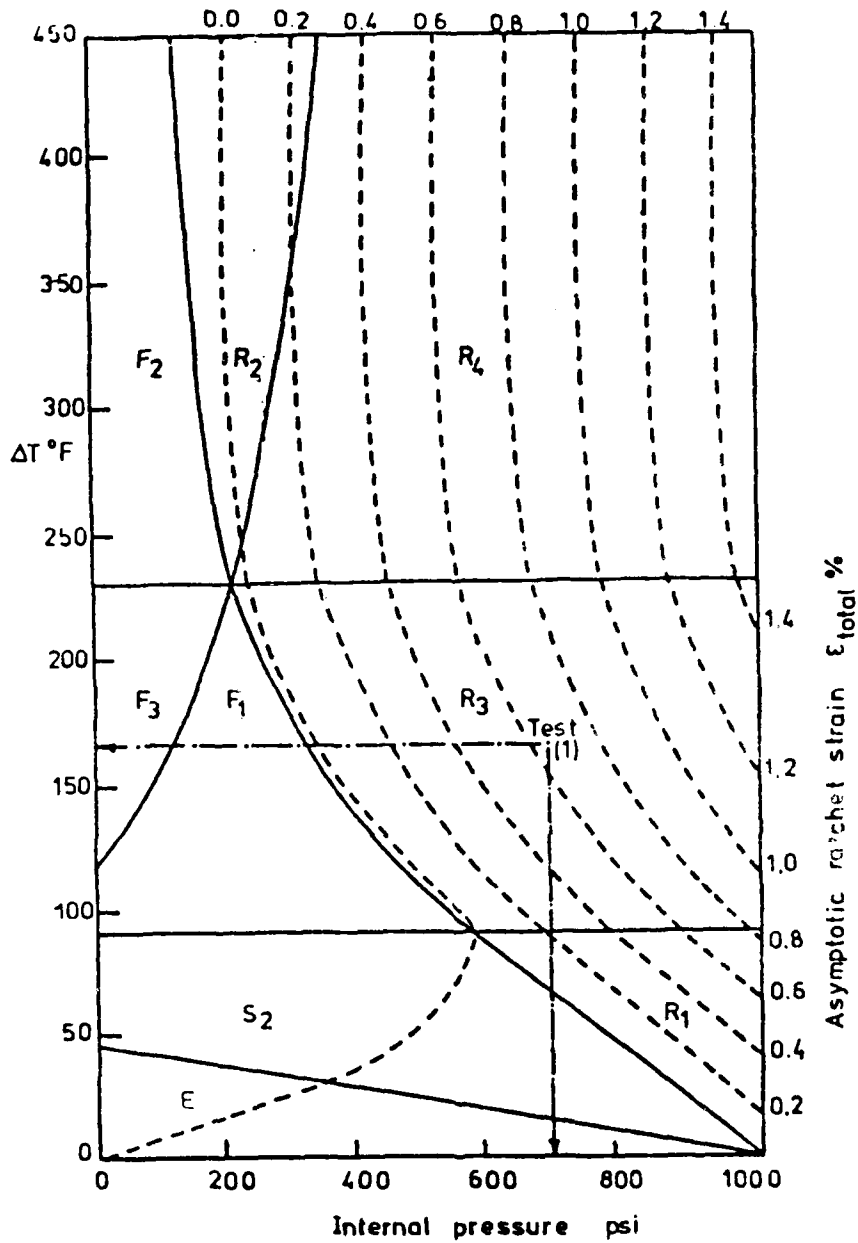


Fig.7. Full solution map and contours of total ratchet strain for a tube with $D/t=21.51, h=0.328$ using monotonic properties of 304 SS at 900 F ($\sigma_y=111.5 \times 10^3$ psi, $E=23.3 \times 10^6$ psi, $\alpha=11 \times 10^{-6}/F$, $K=38.56, \nu=0.3$)

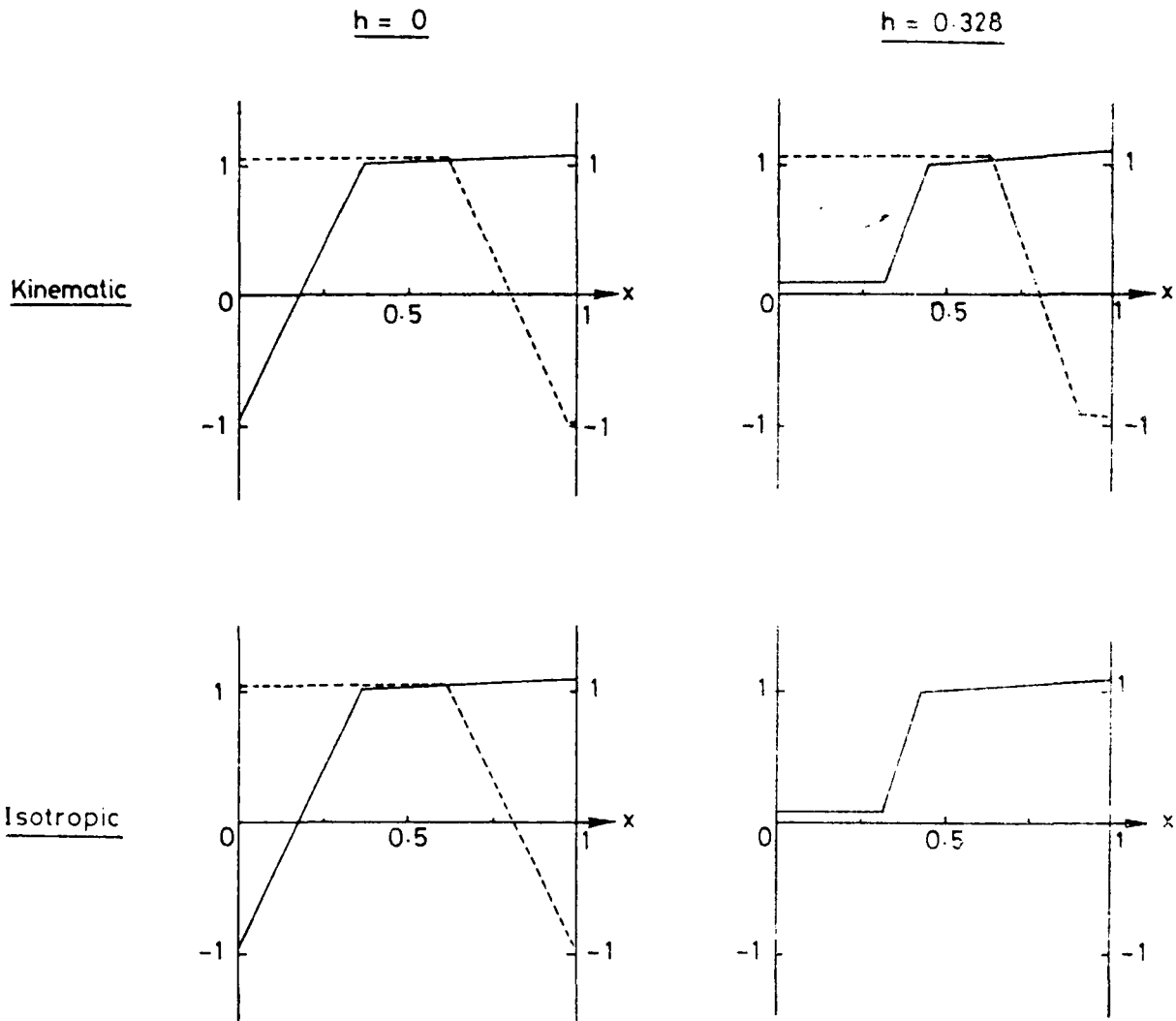


Fig. 8a Stress distribution during first cycle as obtained numerically for $h = 0$ and $h = 0.328$ for both kinematic and isotropic hardening rules, for $\sigma_p = 0.675 \sigma_y$ and $\sigma_t = 2.74 \sigma_y$ for 304 SS.

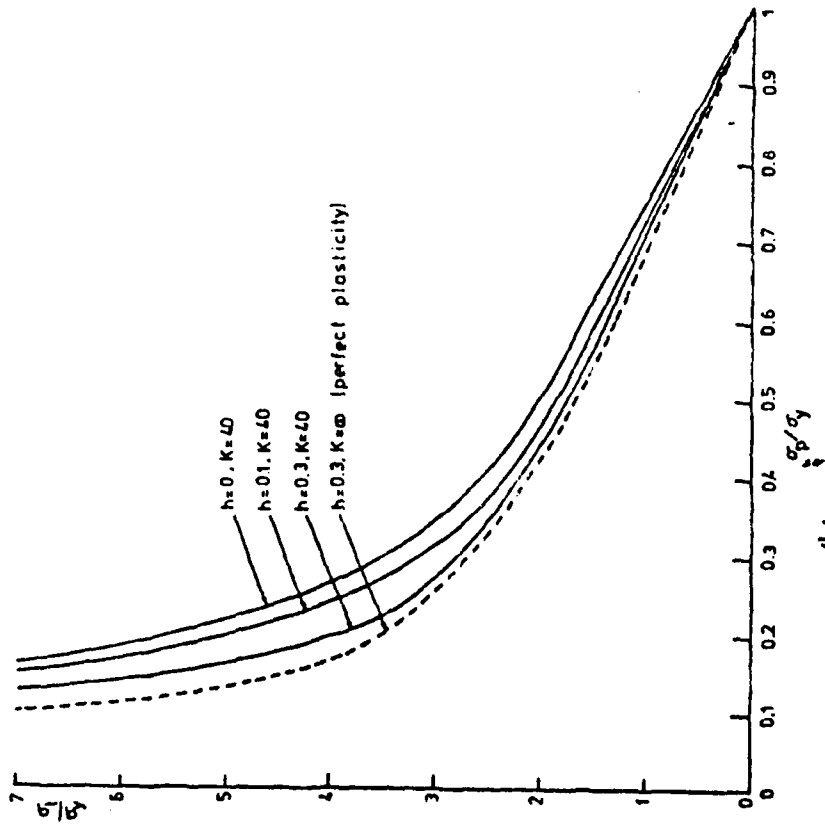
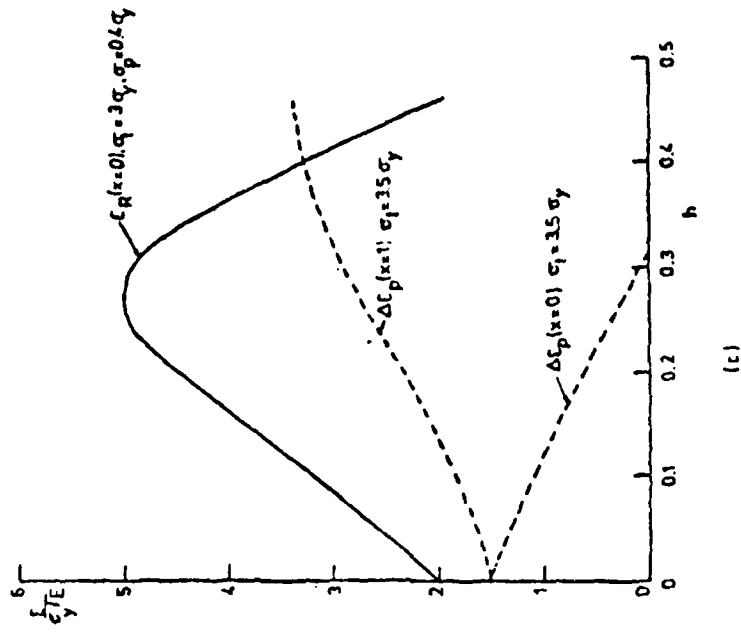


Fig 8 b) Effect of h on ratchet boundary



c) Effect of h on ratchet strain and amplitudes of cyclic plasticity

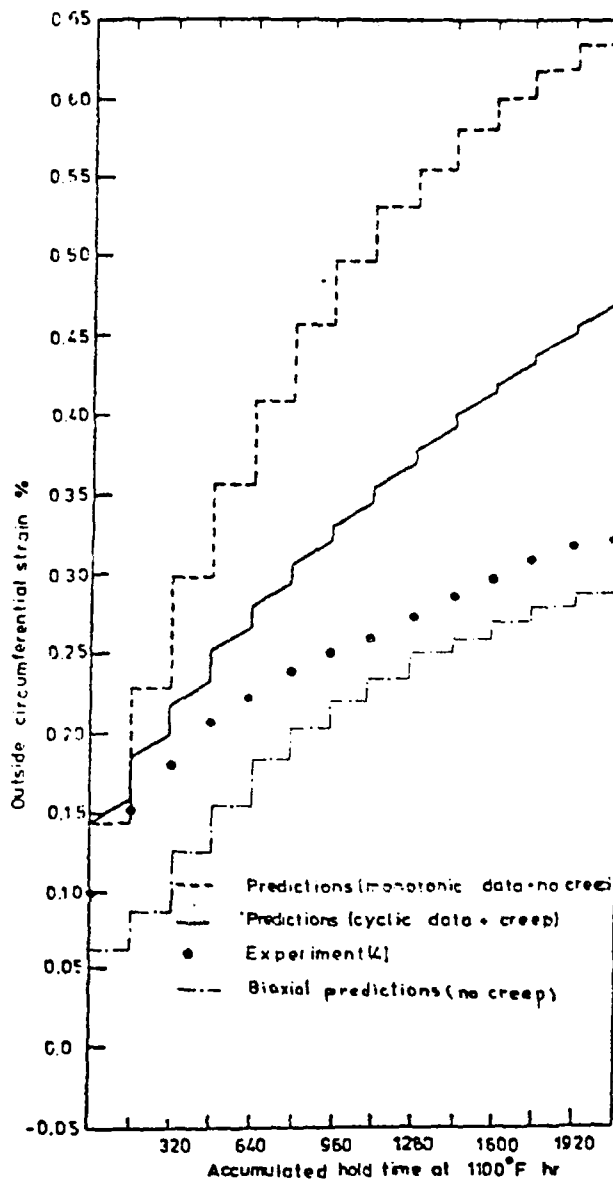


Fig 9 Comparison between model predictions and experimental results for test 1

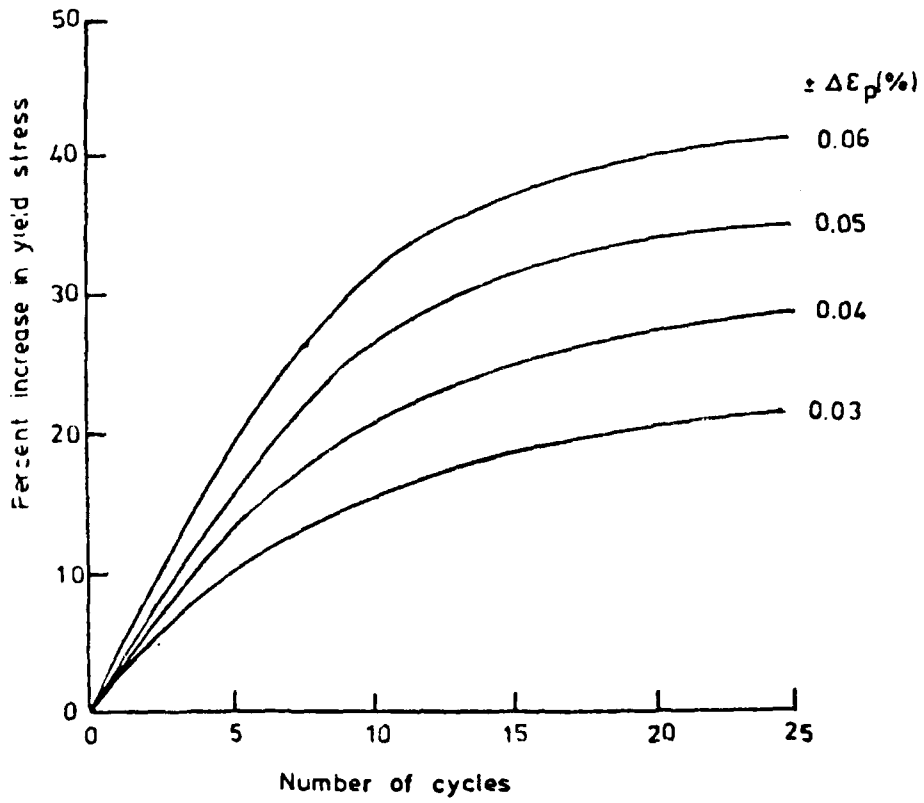


Fig 10 Characterization of cyclic hardening in 304 SS

PART 2

KINEMATIC HARDENING ANALYSIS OF RATCHET

STRAIN IN THE "PULLEY TEST"

Abstract

The classical Bree problem-which represents an uniaxial model of a thin tube subjected to combined internal pressure and cyclic thermal stress across its wall-can be simulated by means of the pulley test in which a wire or strip specimen is subjected to combined steady tensile stress and cyclic bending stress. In this paper, accumulation of ratchet strain in the pulley test is investigated using a linear kinematic hardening material model from which perfect plasticity can be generated as a special case. The results of the investigation show that asymptotic ratchet strains are linearly related to the excess in mean stress σ_p above its value σ_p^* at the ratchetting limit regardless of the thermal stress amplitude. Comparisons with test results on copper wire specimens-which exhibit non-linear hardening rate-confirm the qualitative validity of this simple relation. Deviations between theory and experiment are attributed to metallic cyclic creep. Further, perfect plasticity results are shown to be well predicted by a linearized lower bound estimate.

1. INTRODUCTION

Incremental strain growth (or ratchetting) and low cycle fatigue damage can be major causes of failure of mechanical components subjected to cyclic thermal loading. One of the common ratchetting problems in power

generation industries is that of a thin-walled pipe subjected to combined internal pressure and cyclic thermal gradient across its wall which is known as the "Bree problem" [1]. Testing of such components under realistic thermal conditions usually involves prohibitive cost in terms of equipment and strain measuring devices [2,3]. Such difficulties have motivated the development of simpler tests in which cyclic thermal stresses are simulated by means of cyclic bending. This is achieved by what is termed as the "pulley test" [4,5,6] in which a wire or a strip specimen of the material whose behaviour is to be investigated is cyclically bent around the circumference of a freely rotating pulley while subjected to steady tensile load as illustrated in Fig. (1a). Considering the segment ABC where $AB=BC=\pi\rho$ and ρ is the radius of the pulley, when the dead weights W are in position (1), AB is subjected to combined tension and bending while BC is subjected to tension only. Alternatively, when the dead weights are moved to position (2), BC will be subjected to combined tension and bending while AB is subjected to tension only. In this manner, the cyclic vertical movement of the dead weights brings about a combination of steady tension and cyclic bending in segments AB and BC of the specimen. The interaction between elastic and plastic strains during this loading cycle causes incremental strain growth which manifests itself in cyclic lengthening of the specimen.

The pulley test has been utilized by Megahed et al [4] as a simple test by which the concepts of ratcheting and shakedown can be illustrated experimentally. Figure (1b) shows a sample of the results obtained for the cyclic strain growth of copper wire specimens. It is seen that the observed behaviour resembles to a great extent the ordinary creep behaviour, i.e. an initial primary stage followed by a secondary stage of constant

cyclic strain rate. The prediction of observed steady state rates by means of rapid cycle solutions has been discussed by Meqahed et al [5]. Ng [6] conducted ratchetting tests on thin strip specimens using a pulley apparatus to investigate the behaviour of 316 stainless steel at room and elevated temperatures.

In this paper, theoretical solutions for the development of primary ratchet strain in both wire and strip specimens are generated using the kinematic hardening plasticity theory. This theory has the advantage of simulating the Bauschinger effect observed in many metals but lacks the capability of reproducing the cyclic phenomena of metals, viz, cyclic hardening, cyclic creep and cyclic relaxation which have a pronounced influence on the behaviour of structural components subjected to cyclic loading [7]. However, the solutions presented here provide an estimate of cyclic strain growth as predicted by a classical theory of plasticity commonly employed in many inelastic finite element packages [8].

2. THE EQUIVALENT BREE PROBLEM

Elastic bending stresses which arise in a specimen of thickness d bent around a pulley of radius ρ are given by $\pm \sigma_t$ where $\sigma_t = Ed/2\rho$. The stress variation along the thickness of the specimen is given by:

$$\sigma(x) = \sigma_p + \sigma_t (2x-1) \quad (1)$$

where σ_p is the direct tensile stress due to dead weights and x is a dimensionless position variable along the thickness d with $x = 0$ at the point of specimen contact with the pulley and $x = 1$ at the most outer fiber (Fig. 2a). It is clear therefore that the cyclic vertical travel of the dead weights gives rise to a cyclic elastic stress field which varies between

$\sigma(x) = \sigma_p$ and $\sigma(x) = \sigma_p + \sigma_t (2x-1)$. It can be shown that an equivalent problem-which produces the same cyclic stress field as above-is that of an assembly of infinite number of bars which are allowed to deform in the axial direction only under the combined effect of a uniform tensile stress σ_p and a cyclic thermal strain $\epsilon^{th}(x)$ which cyclically varies between $-2\sigma_t \cdot x/E$ and zero (Fig.2b). In the multi-bar assembly, the constant total strain is the sum of elastic and thermal strain components, i.e. $\epsilon(x) = \sigma(x)/E - 2\sigma_t \cdot x/E = \text{constant} = C$ which gives the stress history $\sigma(x) = EC + 2\sigma_t \cdot x$. The equilibrium condition is $\int_A \sigma(x) dA = \sigma_p \cdot A_0$ where A_0 is the cross-sectional area of the specimens and dA is the area of a bar at the relative position x . Note that $A_0 = 1$, $dA = dx$ for a strip specimen of unit width and $A_0 = \pi/4$, $dA = 2\sqrt{x(1-x)} \cdot dx$ for a wire specimen of unit diameter (Fig.2c). The constant total strain C can be obtained by satisfying the above condition of equilibrium and the elastic stress field $\sigma(x)$ is obtained as $\sigma(x) = \sigma_p + \sigma_t \cdot (2x-1)$ which is the same as eq. (1). Upon removal of thermal strain, $\sigma(x)$ becomes equal to σ_p .

3. MODES OF CYCLIC PLASTIC BEHAVIOUR

In the elasto-plastic solution, a linear flow rule and a kinematic hardening rule are employed. Thus, plastic strain increments are given by

$$d\epsilon^p = \frac{K}{E} d\sigma \quad (2)$$

where $K = (1-\beta)/\beta$ and βE is the slope of the linearized plastic portion of the stress-strain curve. The kinematic hardening rule implies that the size of the yield surface remains constant at $2\sigma_y$ while its center changes continuously due to plastic deformation.

Upon the application of thermal strain $\epsilon^{th}(x)$ for the first time (first cooling), the resulting elastoplastic stress field in the multi-bar assembly may involve tensile yielding at the outer fibers (Fig.3a) or both tensile yielding at the outer fibers and compressive yielding at the inner fibers (Fig.3b). For the case shown in Fig. (3a), the stress-strain relations are given by:

$$\begin{aligned} \epsilon_1 &= [\sigma_1(x) - 2\sigma_t \cdot x] / E & \text{for } 0 \leq x \leq a_1 \\ \epsilon_1 &= [\sigma_1(x) - 2\sigma_t \cdot x + k(\sigma_1(x) - \sigma_y)] / E & \text{for } a_1 \leq x \leq 1 \end{aligned} \quad (3)$$

where a_1 is the elasto-plastic interface. Since $\sigma_1(a_1) = \sigma_y$, the total strain ϵ_1 is therefore given by:

$$\epsilon_1 = [\sigma_y - 2\sigma_t \cdot a_1] / E \quad (4)$$

substituting ϵ_1 in eq. (3) provides the stress field $\sigma_1(x)$ which upon insertion in the equilibrium condition and evaluating the resulting integrals yields the following expressions for a_1 :

$$\frac{16K}{3\pi} \chi(a_1) = (K+1) \frac{\sigma_y - \sigma_p}{\sigma_t} - \frac{K+2}{2} (2a_1 - 1) \quad (5a)$$

for the wire specimens where the function $\chi(a)$ is defined by:

$$\chi(a) = [a(1-a)]^{3/2} + 16(2a-1) [\sin^{-1}(2a-1) + 2(2a-1) \cdot \sqrt{a(1-a)}] / 3 \quad (6)$$

and,

$$a_1 = [-1 + \sqrt{(1+k)[1+k \sigma_y / \sigma_t \cdot (1 - \sigma_p / \sigma_t)]}] / K \quad (5b)$$

for the strip specimen.

Equations (5a) and (5b) can be used to determine the operating conditions (σ_p, σ_t) which give rise to a given state of deformation. For example fully elastic behaviour (which is equivalent to $a_1 \geq 1$) will occur if $\sigma_p + \sigma_t \leq \sigma_y$, which could be easily verified from Fig. (2a). Also, compressive yielding will commence at $x = 0$ if $\sigma_1(0)$ obtained from eq. (3) becomes less than $-\sigma_y$. This condition is equivalent to $a_1 \leq \sigma_y/\sigma_t$ which upon substitution in eqs. (5a) and (5b) yields

$$\frac{16K}{3\pi} \chi \left(\frac{\sigma_y}{\sigma_t}\right) \geq \frac{K+2}{2} - \frac{(1+k) \sigma_p + \sigma_y}{\sigma_t} \quad (7a)$$

for the wire specimen and,

$$\left(\frac{\sigma_t}{\sigma_y}\right)^2 + [K+1] \left(1 - \frac{\sigma_p}{\sigma_y}\right) \cdot \frac{\sigma_t}{\sigma_y} - K \leq 0 \quad (7b)$$

for the strip specimen. Equations (7a,b) define the locii of operating conditions corresponding to the limiting state between the two stress fields shown in Figs. (3a,b).

Analysis of the stress field shown in Fig. (3b) is dealt with in a similar manner to above. The stress-strain relation are given by:

$$\begin{aligned} \epsilon_1 &= [\sigma_1(x) - 2\sigma_t \cdot x + K(\sigma_1(x) + \sigma_y)]/E \quad \text{for } 0 \leq x \leq b_1 \\ \epsilon_1 &= [\sigma_1(x) - 2\sigma_t \cdot x]/E \quad \text{for } b_1 \leq x \leq a_1 \\ \epsilon_1 &= [\sigma_1(x) - 2\sigma_t \cdot x + K(\sigma_1(x) - \sigma_y)]/E \quad \text{for } a_1 \leq x \leq 1 \end{aligned} \quad (8)$$

Noting that $\sigma_1(b_1) = -\sigma_y$ and $\sigma_1(a_1) = \sigma_y$, it follows that;

$$\epsilon_1 = [\sigma_y - 2\sigma_t \cdot a_1]/E = - [\sigma_y + 2\sigma_t \cdot b_1]/E \quad (9)$$

Note that the width of the elastic core $a_1 - b_1 = 1 - \sigma_y / \sigma_t$. The plastic fronts a_1 and b_1 can be determined from the following relations:

$$\frac{16K}{3} [\chi(b_1) - \chi(a_1)] = (K+1) \frac{\sigma_p}{\sigma_t} - \frac{\sigma_y}{\sigma_t} \quad (10a)$$

for the wire specimen and

$$b_1 = \frac{\sigma_t / \sigma_y + (K+1)(1 - \sigma_p) + K \sigma_y / \sigma_t}{2[\sigma_t / \sigma_y + K]} \quad (10b)$$

for the strip specimen.

Incremental strain growth or ratcheting will take place only if the center line of the specimen ($x=0.5$) experiences tensile plastic deformation due to first cooling. Corresponding operating condition can therefore be determined by imposing the condition $a_1=0.5$ on the above results. This procedure defines the ratchetting limits as:

$$\frac{\sigma_p}{\sigma_y} + \frac{2}{3\pi} \frac{K}{K+1} \frac{\sigma_t}{\sigma_y} \leq 1 \quad \text{for } \sigma_t \leq 2\sigma_y \quad (11a)$$

$$(K+1) \frac{\sigma_p}{\sigma_t} - K \frac{\sigma_y}{\sigma_t} \leq \frac{16K}{3\pi} [\chi(0.5 - \sigma_y / \sigma_t) - \chi(0.5)]$$

$$\text{for } \sigma_t \geq 2\sigma_y \quad (11b)$$

for the wire specimen and,

$$\frac{\sigma_p}{\sigma_y} + \frac{1}{4} \frac{K}{K+1} \frac{\sigma_t}{\sigma_y} \leq 1 \quad \text{for } \sigma_t \leq 2\sigma_y \quad (12a)$$

$$\frac{\sigma_p \cdot \sigma_t}{\sigma_y^2} - \frac{1}{K+1} \frac{\sigma_t}{\sigma_y} \leq \frac{K}{K+1} \quad \text{for } \sigma_t \geq 2\sigma_y \quad (12b)$$

for the strip specimen. Operating conditions which satisfy eqs. (11a, 12a) will give rise to elastic shakedown (regions S1, S2) and those which satisfy

eqs (11a,12b) give rise to reversed plasticity region F) as shown in the interaction or Bree diagram of Fig.(4). The steady tensile stress which defines the ratchetting limit as determined from the above inequalities is denoted by σ_p^* . Note that ratchetting limits corresponding to perfect plasticity material (Fig.4b) can be generated from the above results by letting $K \rightarrow \infty$. This yields the familiar results of Bree [1] for the strip specimen and the analogous results for a circular Bree element. It is noted that the ratchetting limits σ_p^* corresponding to perfect plasticity do not differ considerably from kinematic hardening solution for $K = 50$ (Fig. 4a) which is characteristic of many strain hardening materials.

4. ACCUMULATION OF RATCHET STRAIN

a. Kinematic Hardening Solution

Elasto-plastic analysis of loading cycles subsequent to the first cooling shows that ratchet strain accumulates by means of two distinct mechanisms denoted as R_1 and R_2 (Fig. 4a). The ratchetting mechanism R_1 operates at $\sigma_t < 2\sigma_y$ as well as during the initial phase of the intermediate regime $R_1 \rightarrow R_2$. The mechanism R_2 operates at $\sigma_t > 2\sigma_y$ as well as the second phase of regime $R_1 \rightarrow R_2$. Defining a typical cycle N by the $(n-1)$ th cooling and n th heating half cycles, where $n=2N$. Figure (5a) shows the cyclic stress field present during the N th transient cycle and the steady state of the mechanism R_1 and Fig. (5b) shows the analogous stress field for mechanism R_2 . It is seen that R_1 will invariably exhibit tensile yielding which takes place in the fibers $a_{n-1} < x < 1$ during cooling and in the fibers $0 < x < a_n$ during heating. The analysis shows that $a_{n-1} < 0.5 < a_n$ during the transient stage but as cycling continues both a_n and a_{n-1} approach the value of 0.5 at the

steady state. Figure (6) summarizes the results obtained from the elasto-plastic analysis of the ratchetting mechanisms. It is shown that the plastic strain increment during the Nth cycle δ_N is given by:

$$\delta_N = (a_n - a_{n-1}) \cdot 2\sigma_t/E \quad (13)$$

Hence, $\delta_N \rightarrow 0$ at the steady state and the behaviour approaches an elastic shakedown state.

In regime R2, the cyclic stress field exhibits both tensile and compressive yielding during each half cycle as shown in Fig.(5b). Again at the steady state ($a_n = a_{n-1} = 0.5$), $\delta_N \rightarrow 0$ and the plastic fronts corresponding to compressive yielding b_n and b_{n-1} approach $0.5 + \sigma_y/\sigma_t$, $0.5 - \sigma_y/\sigma_t$ respectively. Thus, the behaviour at the stationary state is that of a reversed plasticity at the inner and outer fibers of the assembly and there will be an associated elastic core of width $2\sigma_y/\sigma_t$. The spatial variations of plastic strain at the stationary state are illustrated in Fig.(5). It is clear that the cyclic reduction in the increment of ratchet strain is due to strain hardening and the presence of cyclic plasticity above $\sigma_t = 2\sigma_y$ is due to the employment of the kinematic hardening rule. In the intermediate regime $R_1 \rightarrow R_2$, the behaviour changes from R_1 to R_2 when sufficient hardening has evolved such that reverse yielding in compression starts to take place.

The manner by which the final results are presented in Fig.(6) is very convenient for computer programming. These results have been used to determine the cyclic accumulation of ratchet strain for operating conditions representative of the three regimes; R_1 , R_2 and $R_1 \rightarrow R_2$ as shown in Fig.(7). For $K = 50$, which is characteristic of many alloy steels, the behaviour approaches a steady state in about 50 cycles. The computer program has also been used to generate the contours of the asymptotic values of ratchet strain $\epsilon^p(0.5)$ in the Bree diagram as shown in Fig.(4a). Further discussions of ratchet

strain contours and their relations with the limit mean stress σ_p^* will be presented in the following section of the paper.

b. Perfect Plasticity Solution

The perfect plasticity solution for the accumulation of ratchet strain can be generated from the kinematic hardening results by letting the strain hardening coefficient $K \rightarrow \infty$. This has the following effects:

1. The intermediate ratchet mechanism $R_1 \rightarrow R_2$ will not be present in the manner described earlier since the switch from R_1 to R_2 is primarily due to strain hardening. Hence, this intermediate regime will involve tensile yielding only in exactly the same manner described earlier for mechanism R_1 employed below $\sigma_t = 2\sigma_y$ as shown in Fig. (4b).
2. Ratchet strain will accumulate in equal increments per cycle and hence total ratchet strain is unbounded as shown in the examples of Fig.(7).

Letting $K \rightarrow \infty$ in the recurrence relations presented in the algorithm shown in Fig.(6) yields the following closed form expressions for ratchet strain in the strip specimen:

$$\begin{aligned} \delta_N &= 2\sigma_t/E. \left[1 - 2 \sqrt{(\sigma_y - \sigma_p)/\sigma_t} \right] && \text{for regime } (R_1) \\ & && (14) \\ \delta_N &= 2\sigma_y/E. \left[\frac{\sigma_p \sigma_t}{\sigma_y^2} - 1 \right] && \text{for regime } (R_2) \end{aligned}$$

which is the familiar result obtained by Bree [1]. The corresponding results for the wire specimen can not be reduced to closed forms and will still have to be programmed.

5. DISCUSSION OF RESULTS AND CONCLUSIONS

The results of ratchet strain accumulation obtained in previous section are now compared with simplified bounding

results [9] as well as experimental observations [5]. The ratchetting limits σ_p^* separate the ratchetting regime from shakedown regime for $\sigma_t \leq 2\sigma_y$ and ratchetting regime from reversed plasticity for $\sigma_t \geq 2\sigma_y$. For perfect plasticity models, Ponter and Cocks [9] derived a linearized relationship between the increase in ratchet displacement per cycle and the increases in mean and cyclic thermal stresses; σ_p, σ_t above the shakedown limit. This result is used to obtain a simple lower bound which for kinematically determinate structures shows that for moderate thermal loading, the cyclic increment of ratchet displacement is greater than four times the elastic displacement of the body if it were subjected only to the increase in mean stress above σ_p^* ; $\Delta\sigma_p = \sigma_p - \sigma_p^*$. This result is strictly correct for loads below the shakedown limit $\sigma_t = 2\sigma_y$. Ponter and Cocks [9] compared the lower bound result with exact solution for the classical Bree problem which is equivalent to the strip specimen in the present work.

Figures (8a,b) compare exact solutions with the linearized lower bound for wire and strip specimens at $\sigma_t = \sigma_y, \sigma_t = 2\sigma_y$ which lie below the shakedown limit ($\sigma_t = 2\sigma_y$) as well as at $\sigma_t = 4\sigma_y, \sigma_t = 6\sigma_y$ which exceeds σ_t^* . The linearized lower bounds at $\sigma_t > \sigma_t^*$ are calculated by excluding the regions of reversed plasticity at the inner and outer fibers. For example, when a strip specimen is subjected to $\sigma_t = 4\sigma_y$, reversed plasticity takes place at the inner fibers $0 \leq x \leq 0.25$ and the outer fibers $0.75 \leq x \leq 1$ and the fibers $0.25 < x < 0.75$ experience elastic deformation only (Fig.5). The lower bound is calculated for an equivalent elastic strip of width = 0.5 and subjected to the original axial force which means that the effective mean stress is doubled. The comparisons shown in Figs. (8a,b) indicate that the lower bounds are quite close to exact solutions except when σ_p approaches σ_y .

Investigations of kinematic hardening predictions of asymptotic ratchet strain at the core of the specimen shows that $\epsilon_{K.h}^P(0.5)$ is linearly related to the excess in σ_p above σ_p^* in the following manner:

$$\epsilon_{k.h}^P(0.5) = K/E \cdot A \sigma_p = K/E \cdot (\sigma_p - \sigma_p^*) \quad (15)$$

at any value of σ_t either below or above $\sigma_t^* = 2\sigma_y$. The dependence of plastic strain on σ_t is implied by the variation of σ_p^* with σ_t . It is interesting to note that the rate of change of plastic strain with respect to σ_p equals the linear strain hardening coefficient K/E . This means that the stress state at the core of the specimen $\sigma(0.5)$ is given by the stress-strain curve of the material. In fact, examination of the stress states at $x = 0.5$ as obtained from the computer program shows that:

$$\sigma(0.5) = \sigma_y + \sigma_p - \sigma_p^* \quad (16)$$

Although the above results are obtained for linear kinematic strain hardening material, analogous results for non-linear hardening can be derived. This may be checked by considering the ratchetting tests conducted by Megahed et al [4,5] on copper wires whose operating conditions and ratchetting limits (σ_t^*) are shown in Fig.(9a). The stress-strain curve of the copper wires exhibits non-linear hardening which can be fitted to the power law;

$$\bar{\epsilon}^P = A(\sigma - \bar{\sigma})^{1/n} \quad (17)$$

where $\bar{\sigma}$ is the elastic limit, A , n are material constants. Hence, the result for $\epsilon^P(0.5)$ which should be applied to non-linear hardening material in an analogous manner to eq.(15) should be:

$$\epsilon^P(0.5) = A (\sigma_p - \sigma_p^*)^{1/n} \quad (18)$$

recalling the sample of observed ratchet strain shown in Fig.(1) and noting that the steady ratchetting rate attained after the initial primary stage is mainly due to cyclic creep phenomena [5], ratchet strain $\epsilon^P(0.5)$ appearing in eq.(18) is

interpreted as the primary ratchet strain component (Fig.10). Figure(9b) shows the experimental primary ratchet strain at three levels of σ_t against $(\sigma_p - \sigma_p^*)$ compared with the stress-strain curve of the material. It is clearly seen that the experimental $\epsilon^P(0.5)$ lie on a single curve which supports the universal dependence of ratchet strain on $\sigma_p - \sigma_p^*$. However, the experimental curve of $\epsilon_p(0.5)^*$ lies above the stress-strain curve of the material and the deviation is attributed to primary cyclic creep [5].

Acknowledgement

The author appreciates the helpful discussions of the present work with Prof. A.R.S. Ponter of Leicester University, England, U.K. This work is partially supported by the European Research Office (ERO) of the U.S.Army.

6. REFERENCES

1. Bree, I., "Elastic-plastic Behaviour of Thin Tubes subjected to Internal pressure and Intermittent High Heat Fluxes with Applications to Fast-Nuclear-fuel Elements," J.Strain Analysis, Vol. 2, No.3, 1967,pp. 226-238.
2. Corum, J.M., et al, "Thermal Ratchetting in Pipes Subjected to Intermittent Thermal Downshocks at Elevated Temperates", 2nd Int.Congress on Pressure Vessels and piping, San Fransisco, California, June, 1975.
3. Yamamoto, S., et al, "Theremal Ratchetting Experiment of Type 304 Stainless Steel pipes under Alternating Cold and Hot Thermal Shocks with Varying Axial Loads," Elevated Temperature Design Symposium, ASME, New York, 1976, p.25.

4. Megahed, M.M., Hayhurst, D.R. and Leckie, F.A., "Cyclic Plastic Behaviour of Structural Components," Int.J.Mechanical Engineering Education, Vo. 10 No.4, 1982, p. 235.
5. Megahed, M.M., Ponter, A.R.S. and Morrison, C.J, "A Theoretical and Experimental Investigation of Material Ratchetting Rates in a Bree Beam Element," to be published in Int.J.Mechanical Engineering Sciences, 1983.
6. Ng, H.W, Ph.D.thesis, University of Liverpool, 1982.
7. Megahed, M.M., Ponter, A.R.S. and Morrison, C.J, "Experimental Investigations into the Influence of Cyclic Phenomeana of Metals on Structural Ratchetting Behaviour " submitted to Int. J. Mechanical Engineering Sciences.
8. Kraus, H., Creep Analysis, John Wiley & Sons, 1980.
9. Ponter, A.R.S. and Cocks, A.C.F. "The Incremental Strain Growth of An Elastic-Plastic Body Loaded in Excess of the Shakedown Limit," University of Leicester, Dept. of Engineering, Report No.82/11.

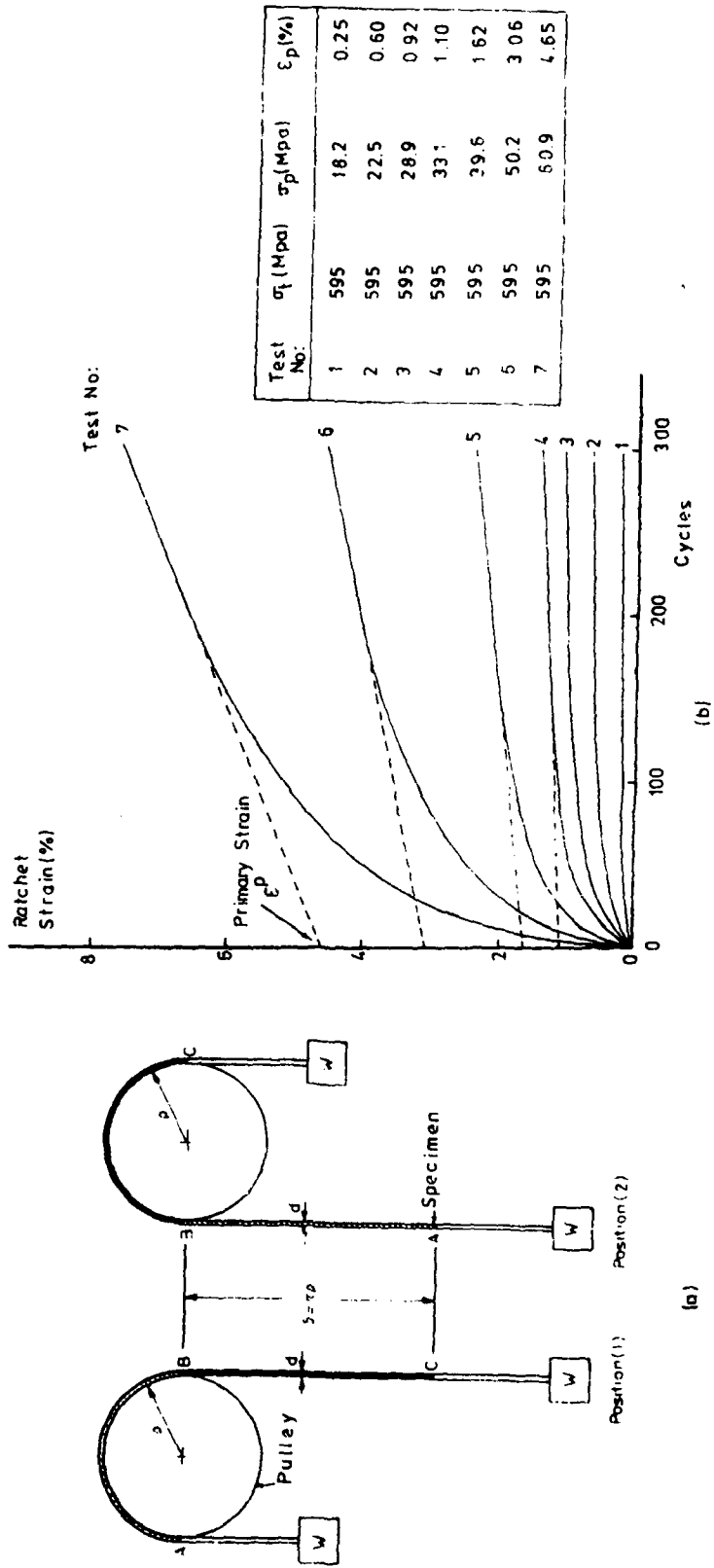


Fig (1) a) Schematic Illustration of the Pulley Test b) Samples of Observed Ratchet Strain

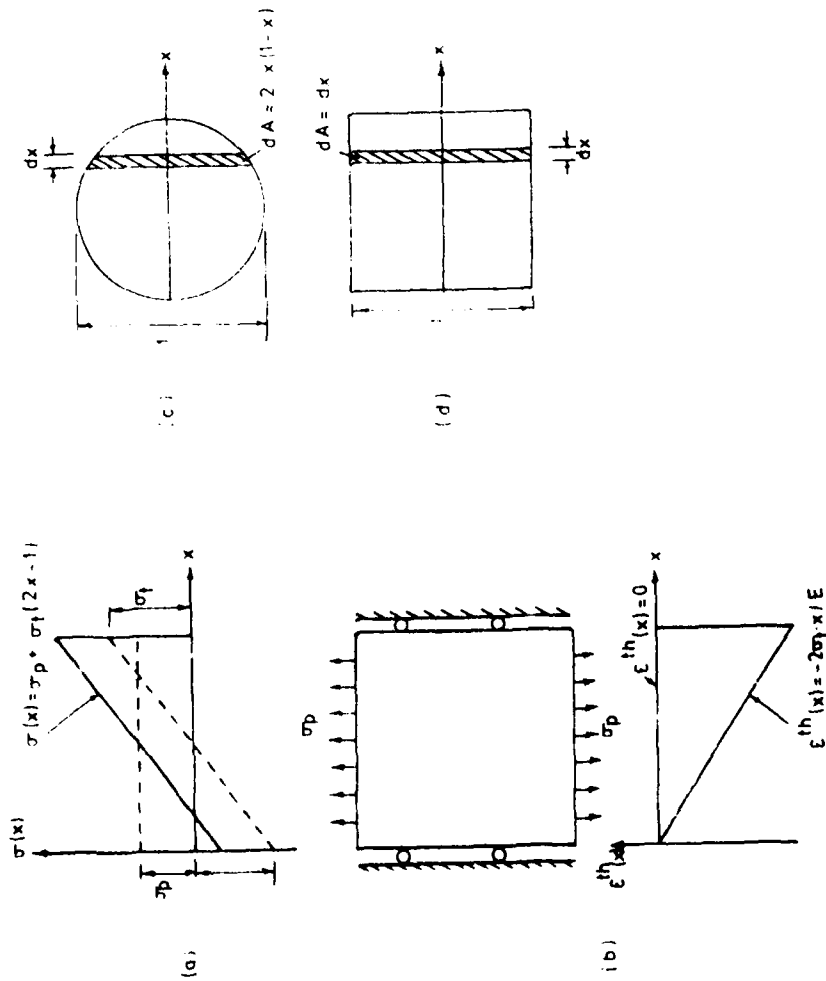
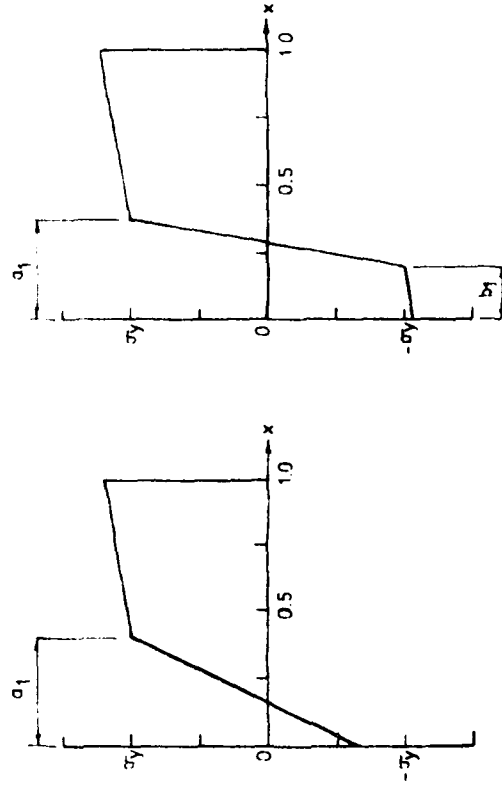
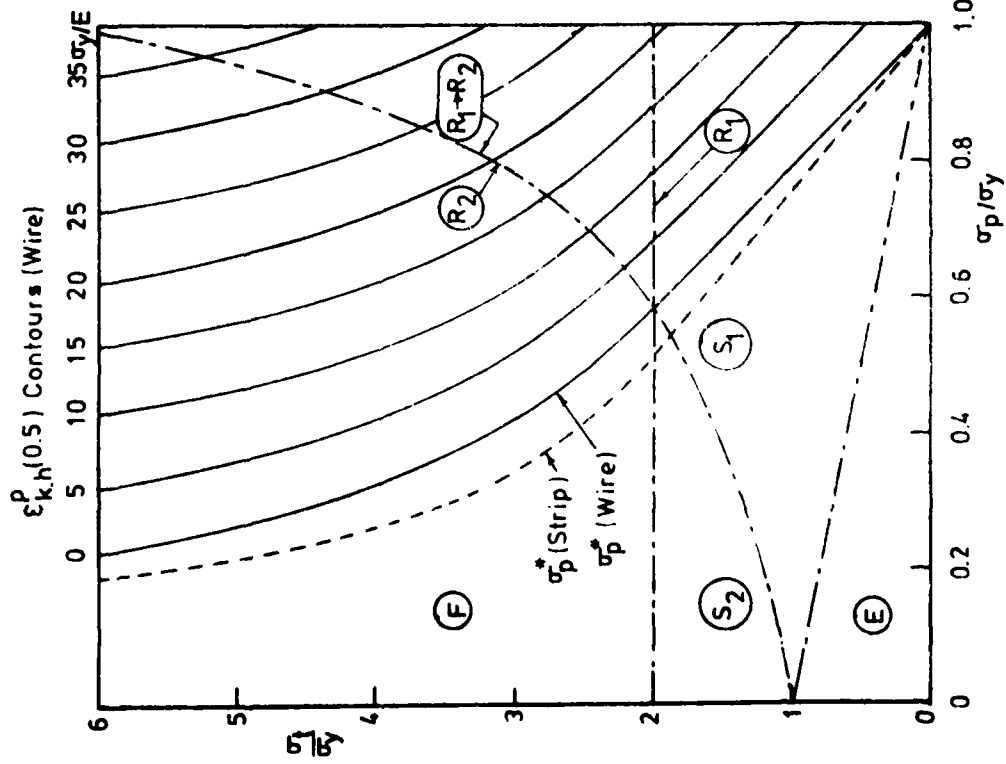
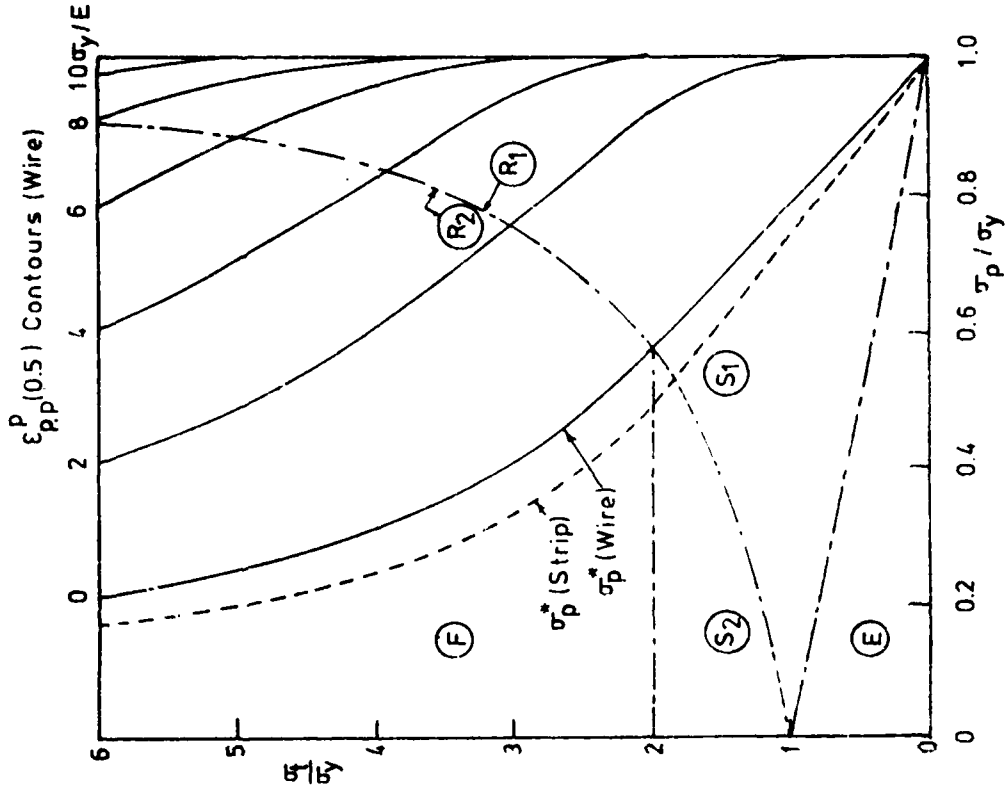


Fig (2) a) Elastic Stress Field b) Equivalent Multi-bar Assembly
 c) Geometry of Wire Specimen d) Geometry of Strip Specimen



(a) Tensile Yielding Only
 (b) Tensile & Compressive Yielding

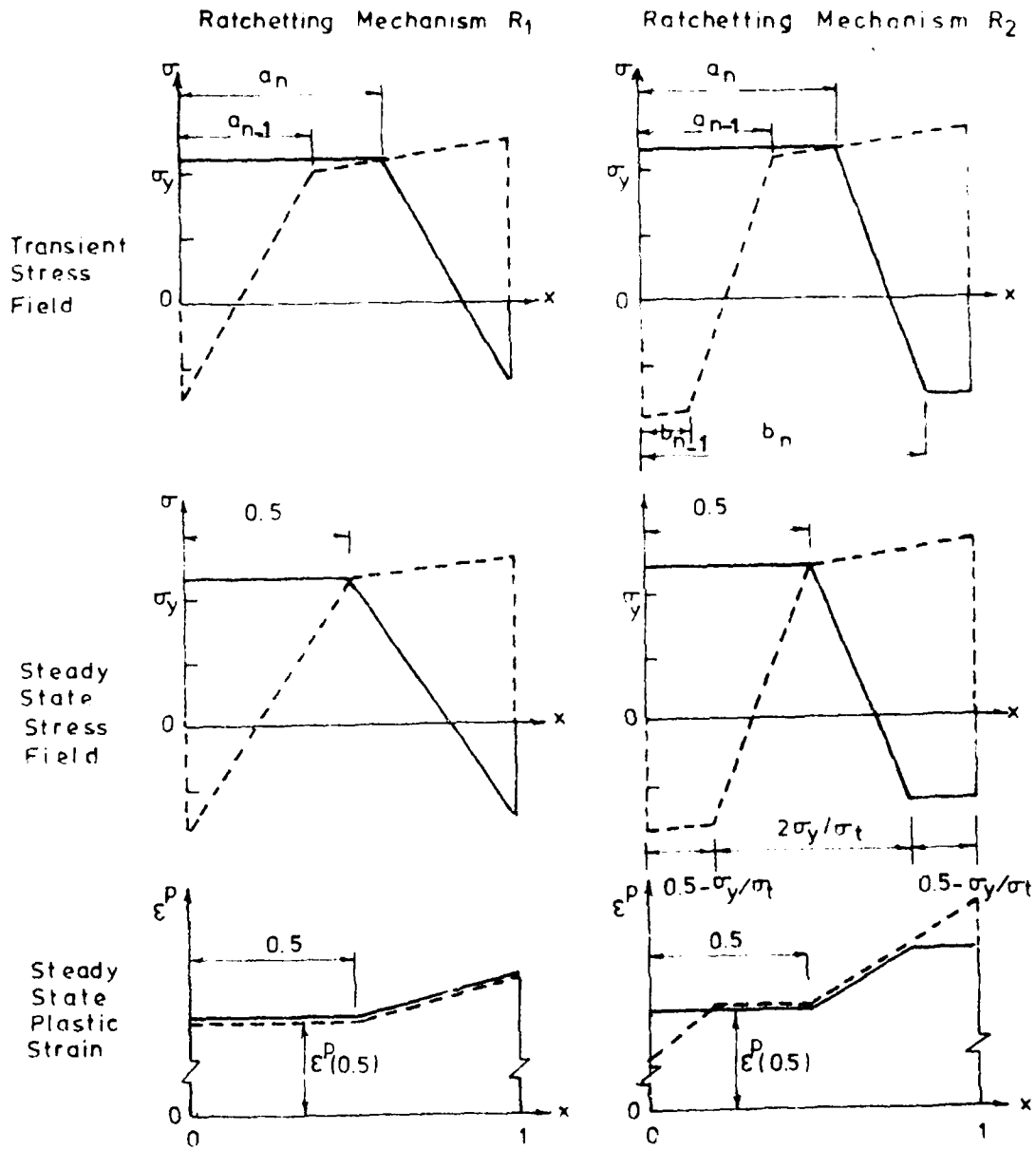
Fig (3) The Two Possible Stress Fields due to First Cooling



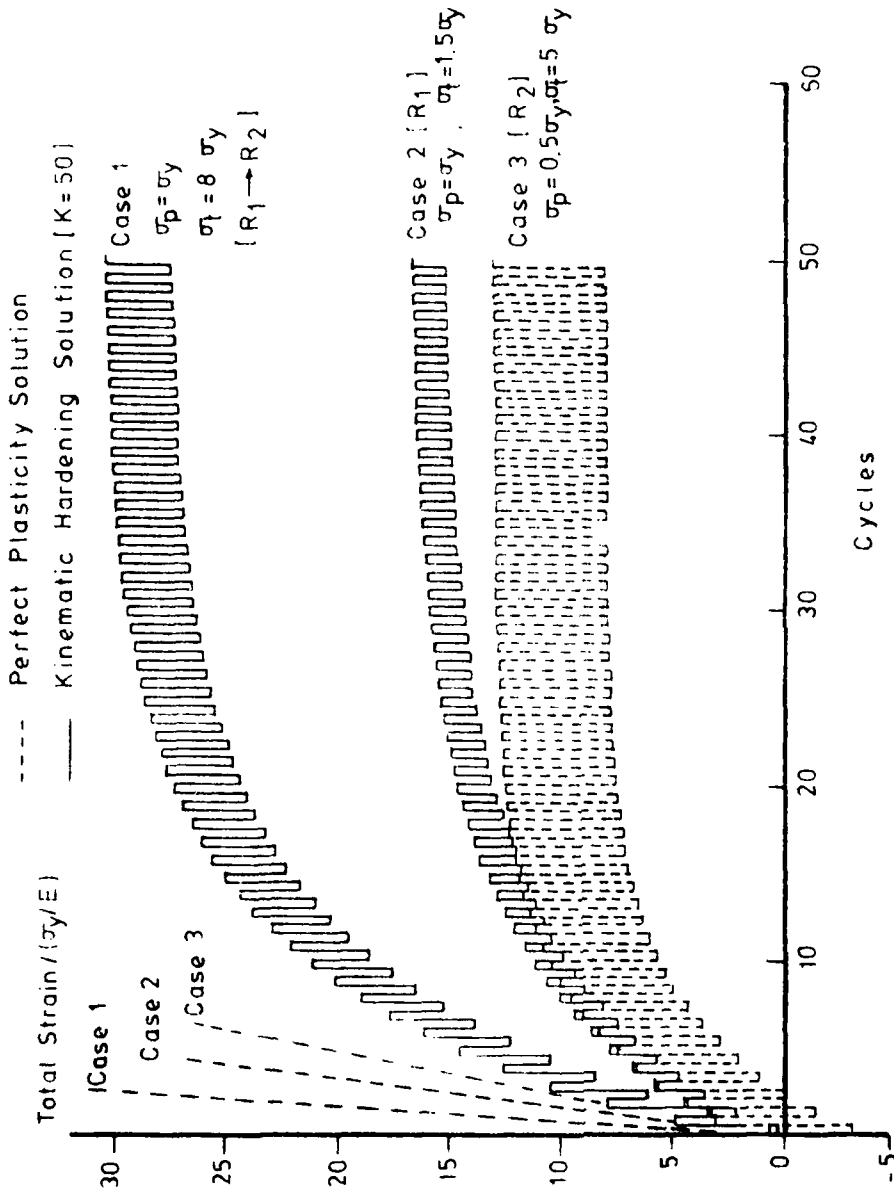
(a) Kinematic Hardening Solution

(b) Perfect Plasticity Solution

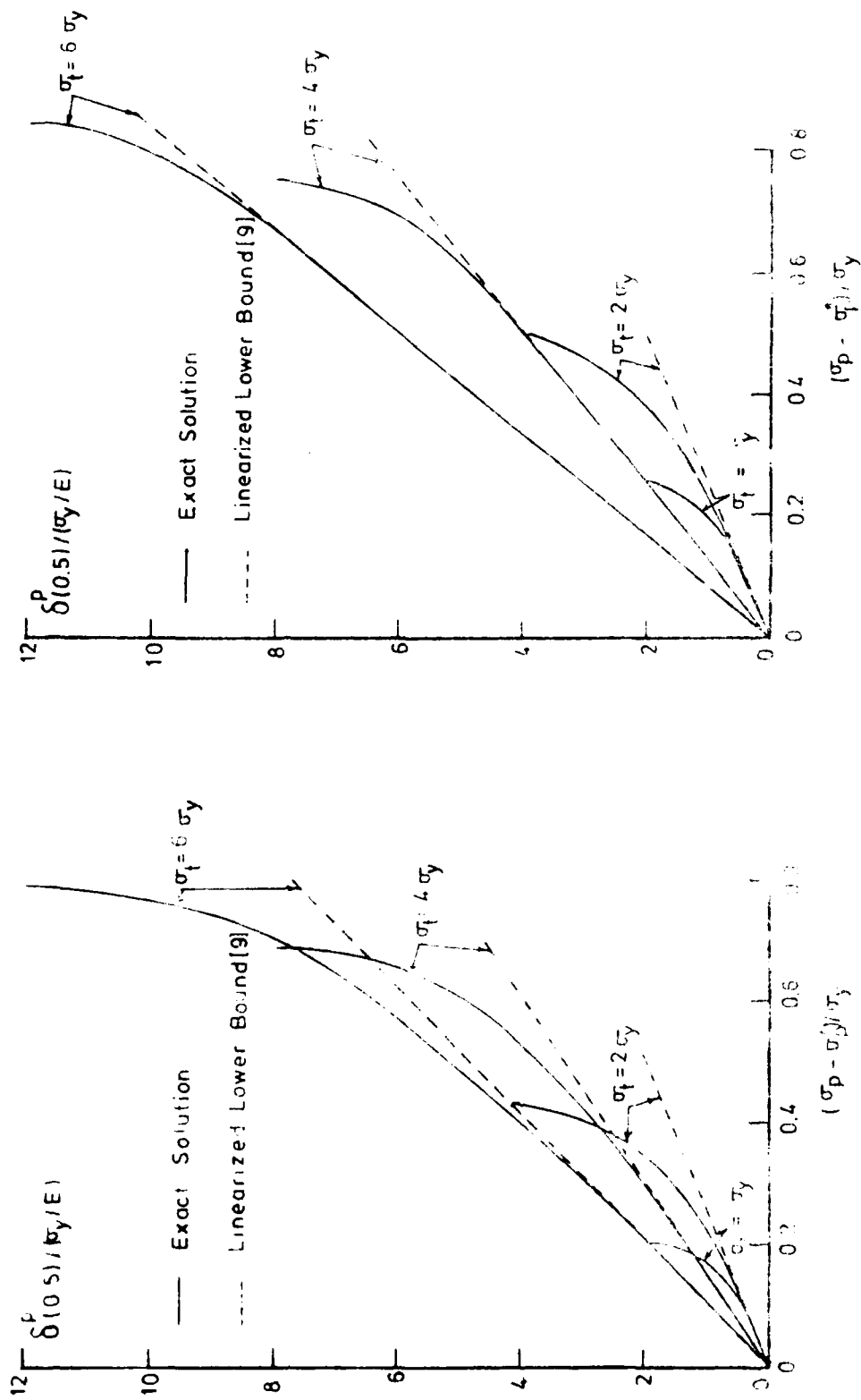
Fig (4) Bree Diagrams and Contours of Ratchet Strains



Fig(5) Transient and Steady State Stress Fields and Plastic Strains for the Ratchetting Regimes



Fig(7) Perfect Plasticity and Kinematic Hardening Solutions for the Accumulation of Ratchet Strain in a Wire Specimen



a) Wire Specimen
 b) Strip Specimen

Fig. 8. Comparison between Exact Perfect Elasticity Solutions for Ratchet Strain per Cycle and Linearized Lower Bound Estimates [9]

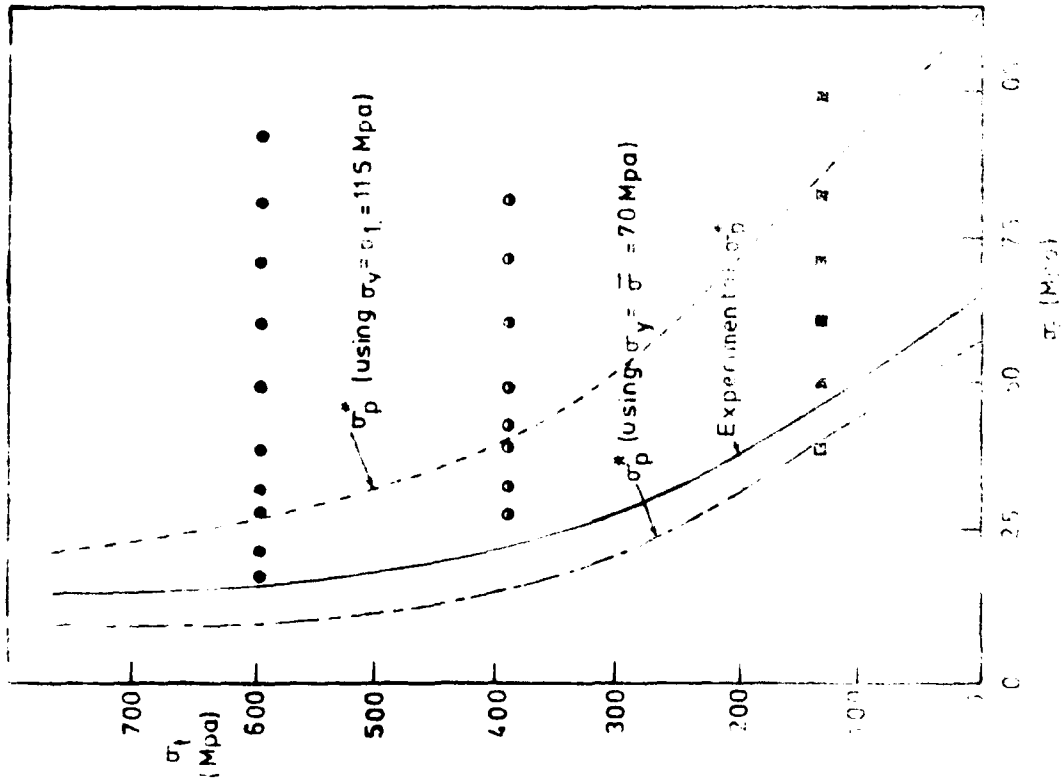
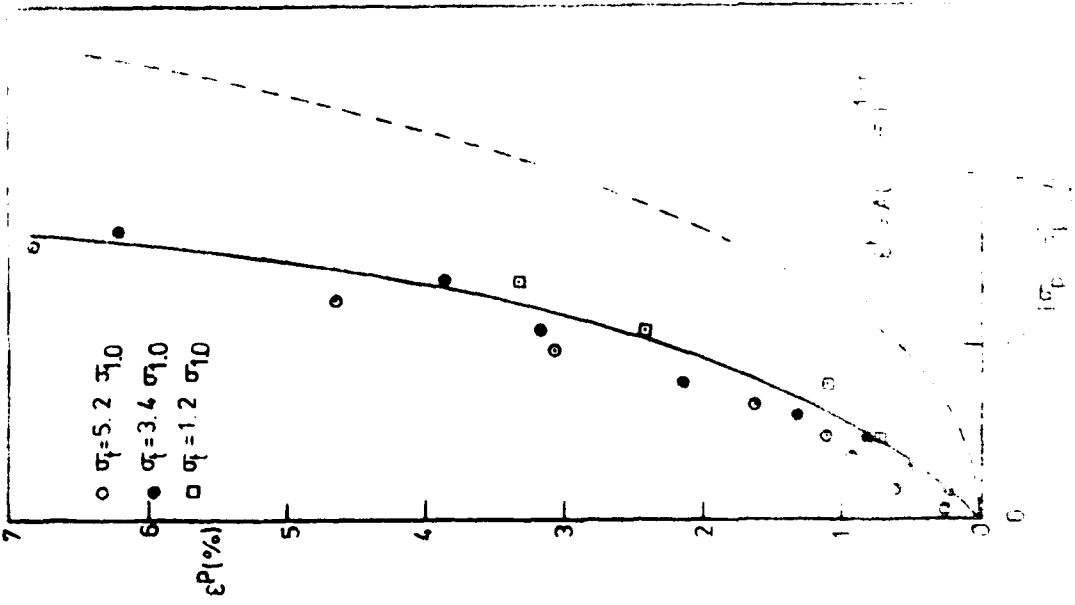


Fig. 9) Operating Conditions and Program for
 Creep Testing of Wires (4) -
 Primary Rate of Creep vs. Primary
 Wire Stress

Fig. 10) Operating Conditions and Program for
 Creep Testing of Wires (4) -
 Primary Rate of Creep vs. Primary
 Wire Stress

PART 3

APPLICATIONS OF REFERENCE STRESS METHOD (RSM)
IN CYCLIC PLASTICITY ANALYSIS

Abstract

The concept of reference stress method (RSM) relies on relating the inelastic deformation behaviour of a structure at a specific point with the behaviour of a uniaxial specimen under reference test conditions. The RSM has proved successful in time-dependent creep analysis since it obviates the need for excessive collection of material data. In this paper, the RSM is applied to evaluate the plastic behaviour of components subjected to cyclic loading conditions where phenomena such as cyclic hardening, cyclic softening, cyclic creep and cyclic relaxation are dominant. Several examples of beams under both uniform and non-uniform bending are discussed. Comparisons between the results of RSM and several independent test results show very close agreement.

1. Reference Stress Method in Creep Analysis

The reference stress method RSM has been under development during the past twenty years as an approximate technique for analysis of creeping structures. Excellent reviews of the RSM may be found in the works of Kraus [1], Ponter [2] and Sim [3]. In order to recapture the basic concepts of the technique, a beam with rectangular cross-section ($b \times 2h$) is considered.

The beam is subjected to steady bending moment M and its material creeps according to Norton's creep law;

$$\dot{\nu} = A \sigma^n \quad (1)$$

Assuming that plane sections remain plane during creep, the strain-curvature relations are;

$$\dot{\nu}(y) = \dot{\kappa} \cdot y = A \sigma(y)^n \quad (2)$$

where $\dot{\kappa}$ is the curvature rate and y is a coordinate along the depth of the beam. Substituting $\sigma(y)$ as obtained from eq. (2) in the equilibrium condition,

$$M = 2b \int_0^y \sigma(y) \cdot y \cdot dy \quad (3)$$

yields the curvature rate $\dot{\kappa}$ as

$$\dot{\kappa} = A \left[\frac{M}{bh^2} \right]^n \cdot \frac{1}{h} \cdot \left[\frac{2n+1}{2n} \right]^n \quad (4)$$

Equation (4) can be rewritten as:

$$\dot{\kappa} = A \sigma_0^n \cdot \frac{1}{h} \cdot f(n) \quad (5)$$

where

$$\sigma_0 = \alpha \cdot \frac{M}{bh^2}, \quad f(n) = \left[\frac{2n+1}{2n \cdot \alpha} \right]^n \quad (6)$$

The function $f(n)$ can be made to be weakly dependent on the creep exponent n by proper choice of the value of α . Considering that $3 \leq n \leq 11$ for most creeping metals and making $f(3) = f(11)$ yields a value of $\alpha = 1.003$. The corresponding values of the function $f(n)$ - as listed in Table (1) - exhibit very little dependence on n . Adopting an average value of $\bar{f} = 1.578$, the curvature rate is written as:

$$\dot{\kappa} = 1.578 \frac{1}{h} \cdot \dot{\nu} \left[1.003 M/bh^2 \right]^2 \quad (7)$$

Table 1 Values of f(n) for beam under pure bending

n	f(n)	\dot{K} [RSM] / \dot{K} [Exact]
3	1.572	1.004
5	1.584	0.996
7	1.584	0.996
9	1.579	0.999
11	1.572	1.004

Hence, the beam curvature rate is obtained directly from the results of a single creep test conducted at a reference stress $\sigma_0 = 1.003 M/bh^2$. The errors involved in the approximate solution are really quite negligible as can be seen from the ratio \dot{K} [RSM] / \dot{K} [Exact] listed in Table (1).

The identification of the reference stress in the above procedure relies on making the function f(n) weakly dependent on the creep exponent n and hence may prove difficult for components which have no exact creep solution. An alternative and effective way for determining σ_0 depends on scaling down the limit load solution corresponding to perfectly plastic material with yield stress σ_y . It can be shown that the ratio σ_0/σ_y equals M/M_L where M_L is the limit bending moment, i.e.

$$\sigma_0/\sigma_y = M/M_L \quad (8)$$

In cases where no exact limit load expression is available, tests on perfectly plastic models of the prototype structures may be utilized.

The RSM has been verified experimentally for beams of both rectangular and tubular sections under both steady and variable loads. Creep of components such as plates, tubes and panels have been studied using the RSM. In the following section, the RSM is applied to analysis of structures made from cyclic hardening material under conditions of repeated load reversals.

2. Cyclic Plasticity Analysis

Initially annealed metals are known to exhibit cyclic hardening when subjected to repeated reversals of load [4]. The hardening rate can be quite large during the first few cycles but decreases continuously until a cyclic steady state is reached early in fatigue life. The steady state of a cyclically hardening metal is characterized by the cyclic stress-strain curve which connects the cusps of settled hysteresis loops obtained at different strain (or stress) amplitudes. The transient cyclic hardening characteristics can be represented by a family of cyclic stress-strain curves which connects the cusps of hysteresis loops at equal number of cycles and different strain amplitudes as shown in Fig.(1) for 99.9% pure copper.

When a structure made from cyclic hardening metal is subjected to repeated load reversals, its behaviour will reflect the hardening characteristics of its material in terms of its load carrying capacity or deformation amplitudes. In order to apply the reference stress method to cyclic plasticity, a simple example of a rectangular beam (bx2h) subjected to cyclic curvature $\pm K$ is considered. It is required to determine the conditions of a reference uniaxial test which can be used to characterize the beam behaviour. The family of cyclic curves shown in Fig. (1) may be represented by

$$\sigma = B \epsilon^m, \quad m = m(N) \quad (9)$$

where N is the number of cycles. Taking the range of $0.1 \leq m \leq 0.5$ which fits the observed hardening, the problem can be solved in a manner analogous to the creep problems. Again assuming that plane sections remain plane and neglecting elastic strains, the moment curvature relation at the instants of curvature reversals is obtained as:

$$M = bh^2 \cdot \frac{2}{m+2} \cdot B (\pm kh)^m \quad (10)$$

which can be written as:

$$M = bh^2 \cdot f(m) \cdot \sigma(\pm \epsilon_0) \quad (11)$$

where

$$\epsilon_0 = \alpha \cdot kh, \quad f(m) = \frac{2}{(m+2)\alpha^m}$$

Enforcement of $f(0.1) = f(0.5)$ yields $\alpha = 0.674$ and the corresponding variation of f with m is as listed in Table (2). Hence the moment curvature relation can be written as

$$M = 0.993 bh^2 \sigma(\pm 0.647 kh) \quad (12)$$

i.e. the bending moment is determined directly from the results of a reference uniaxial test conducted at $\epsilon_0 = \pm 0.647$ times the surface strain (kh).

Table 2: Values of $f(m)$ for beam under cyclic curvature

m	$f(m)$	$M [RSM] / M [Exact]$
0.1	0.995	0.998
0.2	0.992	1.0
0.3	0.991	1.001
0.4	0.992	0.998
0.5	0.995	0.963

Another example of the application of RSM 's provided by considering the cyclic torsion of a solid bar ($rad. = a$, length= L) subjected to repeated reversals of twist angle θ . Assuming the validity of von-Mises relations, the reference strain solution for the twisting moment T is:

$$T = 1.205 a^3 \sigma(+\epsilon_0), \quad \epsilon_0 = 0.426a \theta / L \quad (13)$$

when the structure is subjected to controlled history of prescribed deformation, the reference uniaxial test is conducted under reversed strain conditions. On the other hand, when the structure is subjected to controlled history of prescribed

loads, the reference uniaxial test is conducted under reversed stress conditions. Reference stress relations in the latter case will be similar to those used in creep analysis.

The above results describing cyclic pure bending of beams are utilized to generate solutions for a host of allied beam bending problems, e.g. cantilevers and simply supported beams. The final results are summarized in table (3). The range of $0.1 \leq m \leq 0.5$ is used throughout.

Table 3. Reference Test Solutions in Cyclic Plasticity

Structure	Loading history	Reference stress(or strain)solution
Rectangular beam (bx2h)	$\pm K$ $\pm M$	$M=0.993bh^2 \cdot \sigma [\epsilon_o]$, $\epsilon_o = \pm 0.647kh$ $K=1.557 \frac{1}{h} \cdot \epsilon [\sigma_o]$, $\sigma_o = \pm 1.005M/bh^2$
Solid bar (rad=a, Length=L)	$\pm \theta$ $\pm T$	$T=1.205 a^3 \cdot \sigma [\epsilon_o]$, $\epsilon_o = \pm 0.426\theta/L$ $\theta=2.354L/a \cdot \epsilon [\sigma_o]$, $\sigma_o = \pm 0.829T/a^3$
Cantilever (L) under Tip Load	$\pm \delta$ at tip $\pm P$ at tip	$P=1.158 \frac{bh^2}{L} \cdot \sigma [\epsilon_o]$, $\epsilon_o = \pm 1.966\delta h/L^2$ $\delta=0.483 \frac{L^2}{h} \cdot \epsilon [\sigma_o]$, $\sigma_o = \pm 0.876PL/bh^2$
Cantilever (L) under distributed load	$\pm \delta$ at tip $\pm q$ (uniform)	$q=2.39 \frac{bh^2}{L^2} \cdot \sigma [\epsilon_o]$, $\epsilon_o = \pm 2.804\delta h/L^2$ $\delta=0.331 \frac{L^2}{h} \cdot \epsilon [\sigma_o]$, $\sigma_o = \pm 0.428qL^2/bh^2$
Simple Beam (2L) under central load	$\pm \delta$ at center $\pm P$ at center	$P=2.316 \frac{bh^2}{L} \cdot \sigma [\epsilon_o]$, $\epsilon_o = \pm 1.966\delta h/L^2$ $\delta=0.483 \frac{L^2}{h} \cdot \epsilon [\sigma_o]$, $\sigma_o = \pm 0.438PL/bh^2$

3. Comparison With Test Results

The reference test results are compared with three sets of experimental data for beam bending. The first set of tests are conducted by Oldroyd[5] on rectangular copper beams under pure bending in an attempt to derive the uniaxial stress-strain curve from the moment-curvature curve by use of Nadai's bending formula [6]. Only monotonic loading is considered in the tests. Hence,

a monotonic stress-strain curve and the central deflection vs. end load in a four-point beam bending test are determined as shown in Fig. (2). Application of eq. (13) yields the reference test predictions which are seen to be in close agreement with the results of the bending test.

The second set of test data [7] involves cyclic bending of rectangular beams made from initially annealed 99.9% pure copper until the cyclic steady state is reached. The tests are conducted under repeated reversals of curvature and the bending moment is determined. The reference test calculation are based upon the uniaxial cyclic stress-strain curve. An exact numerical solution for the moment-curvature relation is also determined on the basis of representing the uniaxial cyclic curve by a Ramborg-Osgood relation. Figure (3a) compares the test results with both the reference test predictions and the exact numerical procedure. Very close agreement is obtained. Figure (3b) shows similar calculations for the cyclic twist of a solid circular bar.

The third set of data are conducted on simply supported 304 stainless steel beams subjected to repeated reversals of central load and central deflections at 1100 °F. Ten cycles of load (or deflection) are completed. The experimental results are shown in Fig. (4a,b). The reference test predictions are based on the 10th cycle cyclic curve obtained by connecting the cusps of three hysteresis loops determined at $\pm \epsilon = 0.4, 0.6$ and 1% . The cyclic curve is fitted to a bilinear relation; $\epsilon = \left[\sigma + 4 (\sigma - \sigma_y) \right] / E$ where σ_y is a material yield stress = 10000psi [9]. Using this relation, the reference strain predictions for the central load P after 10 cycles of reversed deflection $\delta = \pm 0.1$ " in a simple beam with $b = 1$ ", $h = 2$ " and $2L = 24$ " gives 5290 lbs as compared with 5480 lbs from the test results. An excellent agreement of less than 4% error. In the second test, a simply supported beam is subjected to ten repeated reversals of central load $p = \pm 2000$ lbs. The references stress prediction for the 10th cycle deflection range gives 0.082" as compared with an experimental deflection of 0.113". A less satisfactory agreement than the deflection controlled test but still may be accepted in view of the smaller plastic strains

involved in the load controlled test. It is interesting to note that the present predictions compare very well with a full transient analysis of the beam problem [9] .

4. Cyclic Creep Analysis

The phenomenon of cyclic creep is the cyclic strain growth observed in metals when subjected to the combined effect of steady and cyclic load components. A closely related phenomenon to cyclic relaxation of stress under the combined effect of steady and cyclic strain components. Plots of cyclic creep strain against cycles are quite similar to the conventional time-dependent creep curve with a primary stage of decreasing strain rate, a secondary stage of constant strain rate and a tertiary stage with increasing rate before the specimen fails due to fatigue. The strain growth is usually accompanied by a hysteresis loop. Hence, the total plastic strain during a typical load cycle is composed from a small reversed component and a drifting growth component [4] .

The steady cyclic rate of strain growth depends on the maximum stress σ^* and the stress amplitude $\Delta\sigma$ of the stress cycle [10] , i.e.

$$\dot{\epsilon}_N = A \sigma^{*n} \cdot \Delta\sigma^{n\gamma} \quad (14)$$

Tests carried out on different grades of commercially pure Copper [10,11] show that the values of n, γ depend largely on the level of σ^* as compared with the material yield stress. For example; $n=3.2, \gamma=0.03$ at $\sigma^*/\sigma_y = (0.5-1)$, $n=4.6, \gamma=0.2$ at $\sigma^*/\sigma_y = 1-1.5$ and $n=18, \gamma=0.3$ at $\sigma^*/\sigma_y = 4$ where σ_y is the 1% yield stress. Hence, it may be generally stated that for the range of maximum stress encountered in design, the values of $2 \leq n \leq 10$ and $0.02 \leq \gamma \leq 0.2$ are acceptable.

The material law in eq. (14) is used here to estimate the effects of cyclic creep on deformations of structures subjected to cyclic loading. The solution is expressed

in a reference stress form. This is achieved through using the so-called rapid cycle solution applied successfully in the analysis of time-dependent creep deformation in components subjected to cyclic loads with short cycle times compared with the material time scale [12]. The technique provides an upper bound on cyclic structural deformation.

In rapid cycle solution, the cyclic stress field in the structure is assumed to be composed from the cyclic linear elastic stress field and a residual stress field which is in equilibrium with zero external forces. The magnitude of the residual stress field is determined by enforcing the compatibility of cyclic strains resulting from the cyclic stress field over a complete cycle of load. The theoretical basis for the rapid cycle solution may be found in ref. [12] and its application to the analysis of cyclic growth of structures are found in ref. [10, 11].

As an example, consider a rectangular beam subjected to the cyclic history of bending moment which varies between M_1, M_2 . The cyclic elastic stress field is:

$$\begin{aligned}\hat{\sigma}^*(y) &= \frac{3}{2} \frac{M_1}{bh^3} \cdot y && \text{during 1st half cycle} \\ \hat{\sigma}^*(y) &= \frac{3}{2} \frac{M_2}{bh^3} \cdot y && \text{during 2nd half cycle} \\ \Delta\sigma(y) &= \frac{3}{4} \frac{M_1 - M_2}{bh^3} \cdot y\end{aligned}\quad (15)$$

Hence the cyclic stress field $\tilde{\sigma}^*$ is assumed as the sum $\hat{\sigma}^* + \rho$ i.e.,

$$\begin{aligned}\tilde{\sigma}^*(y) &= \frac{3}{2} \frac{M_1}{bh^3} \cdot y + \rho(y) && \text{during 1st half cycle} \\ \tilde{\sigma}^*(y) &= \frac{3}{2} \frac{M_2}{bh^3} \cdot y + \rho(y) && \text{during 2nd half cycle}\end{aligned}\quad (16)$$

where $\rho(y)$ is the residual stress field which should satisfy the equilibrium conditions

$$\int_{-h}^h \tilde{\sigma}^*(y) \cdot y \, dy = 0, \quad \int_{-h}^h \tilde{\sigma}^*(y) \cdot dy = 0 \quad (17)$$

Compatibility of cyclic creep strains resulting from $\sigma(y)$ and $\dot{\sigma}(y)$ requires that;

$$A \left[\frac{3}{2} \frac{M_1}{bh^3} \cdot y + \dot{\rho}(y) \right]^n \left[\frac{3}{4} \frac{M_1 - M_2}{bh^3} \right]^{\delta n} = \dot{K}_N \cdot y \quad (18)$$

where \dot{K}_N is the cyclic curvature rate. Hence, $\dot{\rho}(y)$ is given by:

$$\dot{\rho}(y) = \left[\frac{K_N}{A} \right]^{1/n} \left[\frac{1}{\frac{3}{4} \frac{M_1 - M_2}{bh^3}} \right]^{\delta} \cdot y^{(1-\delta n)/n} - \frac{3}{2} \frac{M_1}{bh^3} \cdot y \quad (19)$$

Upon substitution in the equilibrium conditions, \dot{K}_N is obtained as:

$$\dot{K}_N = A \left[\frac{2n+1-n\delta}{3n} \right]^n \cdot \frac{1}{h} \cdot \left[\frac{3M_1}{2bh^2} \right]^n \cdot \left[\frac{3(M_1 - M_2)}{4bh^2} \right]^{\delta n} \quad (20)$$

It is noted that the associated cyclic stress field may possess a singularity at $y=0$ which can be seen from eq. (19) for $n\delta > 1$. The singularity may be overcome by introducing an assumption that the maximum stress at $y=0$ does not exceed an upper limit which may be taken as some multiples of the material yield stress. A similar procedure has been used in ref. [10] in the analysis of ratchet strain rates in a circular Bree element.

The curvature relation, eq. (20), may be expressed as:

$$K_N = A (\alpha_1 \cdot \sigma_{\max}^*)^n (\alpha_2 \Delta \sigma_{\max})^{n\delta} \cdot \frac{1}{h} f(n, \delta) \quad (21)$$

where

$$\sigma_{\max}^* = \frac{3}{2} M_1 / bh^2, \quad \Delta \sigma_{\max} = \frac{3}{4} (M_1 - M_2) / bh^2, \quad f(n, \delta) = \left[\frac{2n+1-n\delta}{3n \cdot \alpha_1 \cdot \alpha_2} \right]^n \quad (22)$$

The values of α_1, α_2 can be chosen for the practical ranges of $2 \leq n \leq 10, 0.02 \leq \delta \leq 0.2$ such that the function f is weakly dependant upon n and δ . Taking $f(2,0.02) = f(10,0.02)$ and $f(2,0.2) = f(10,0.2)$ provides two relations between α_1 and α_2 which yield their respective values as:

$\alpha_1 = 0.592, \alpha_2 = 0.671$. The corresponding variation of f with n, δ does not vary from the mean value $\bar{f} = 1.596$ by more than $\pm 2.8\%$ as shown in table (4). Hence the final result for reference stress solution is:

$$\dot{\epsilon}_N = 1.596 \frac{1}{h} \dot{\epsilon}_N \left[0.671 \sigma_{\max}, 0.592 \Delta \sigma_{\max} \right] \quad (23)$$

Table (4) Values of $f(n, \delta)$ used in cyclic creep of beams

	$\delta = 0.02$	$\delta = 0.1$	$\delta = 0.2$
$n=2$	1.552	1.581	1.612
$n=4$	1.575	1.609	1.640
$n=6$	1.573	1.611	1.638
$n=8$	1.564	1.604	1.627
$n=10$	1.522	1.595	1.619

Note the closeness of coefficients in eq. (23) with those obtained in the case of cyclic plasticity; Table (3).

An analogous result for cyclic creep deflection of a cantilever under an end load which varies between p_1 and p_2 can be easily obtained as:

$$\dot{\delta}_N = 0.466 \frac{L^2}{h} \cdot \dot{\epsilon}_N \left[0.584 \frac{p_1 L}{2bh^2/3}, 0.571 \frac{(p_1 - p_2)L}{4bh^2/3} \right] \quad (24)$$

5. Conclusions

The reference stress method can be applied to analysis of structures made from cyclically hardened materials. The technique is extremely useful during the initial stages of design since it reduces the problem to conducting a single material test.

hardening test at the reference value of stress (or strain) amplitude. The accuracy of the technique has been demonstrated through comparisons with published test results and exact numerical solutions for simple beams. Checks on more complex components such as plates, panels and tubes should be conducted.

The applicability of the RSM to analysis of cyclic creep behaviour of structures is demonstrated by extending the use of the so called rapid cycle solution used in time-dependent creep analysis. Tests on components operating under conditions where cyclic creep is dominant are required. In principle, the RSM can be applied to analysis of structures under cyclic relaxation conditions.

Acknowledgements

This work is partially supported by the European Research Office (ERO) of the U.S. army.

6. References

- 1- Kraus, H., "Reference Stress concepts for Creep analysis," Welding Research Council Bulletin No.227, (June 1977).
- 2- Ponter, A.R.S "Lecture Notes of a course on Creep," University of Leicester, (1979).
- 3- Sim, R.G., "Reference stress Concepts in the analysis of structures during creep", Int. J. Mech. Sci, Vol.12, pp.561-573 (1970).
- 4- Mroz, Z., "An Attempt to Describe the Behaviour of Metals under Cyclic Loading Using a More General Work Hardening Model", Acta. Mech. Vol.7, pp. 199-212, (1969).
- 5- Oldroyd, P.W.J, "Tension Compression Stress-Strain Curves From Bending Tests" J.Strain Analysis, Vol.6, No.4, (1971).
- 6- Nadai, A, "Theory of Flow and Fracture of Solids", McGraw Hill 1963.
- 7- Fenn, O, "Behaviour of Structures Subjected to Cyclic Plastic Deformation" M. Phil. Thesis, University of Leicester, Oct.1979.

- 8- Corum, J.H. and Richardson, M, "Elevated Temperature Tests of Simply Supported Beams and Circular Plates Subjected to time varying loads," 2nd Nat. Congress of Pressure Vessel and piping, San Francisco, June 23-27, (1975).
- 9- Megahed, M.M. and Leckie, F.A, "Cyclic Hardening Analysis of Beams under Cyclic Loading", 2nd MDP Conference, Cairo, pp. 421-428, (1982).
- 10- Megahed, M.M., Ponter, A.R.S. and Morrison, C.J, "A Theoretical and Experimental Investigation of Material Ratchetting Rates in a Bree Beam Element", to be published in Int. J. Mech. Sci. (1983).
- 11- Megahed, M.M, Ponter, A.R.S. and Morrison, C.J, "Experimental Investigation into the Influence of Cyclic Phenomena of Metals on Structural Ratchetting Behaviour", Submitted to Int. J. Mech. Sci (1983).
- 12- Ponter, A.R.S, "The Analysis of Cyclically Loaded Creeping Structures for Short Cycle Times," Int. J. Solids and Structures, Vol.12, pp. 809-825, (1976).

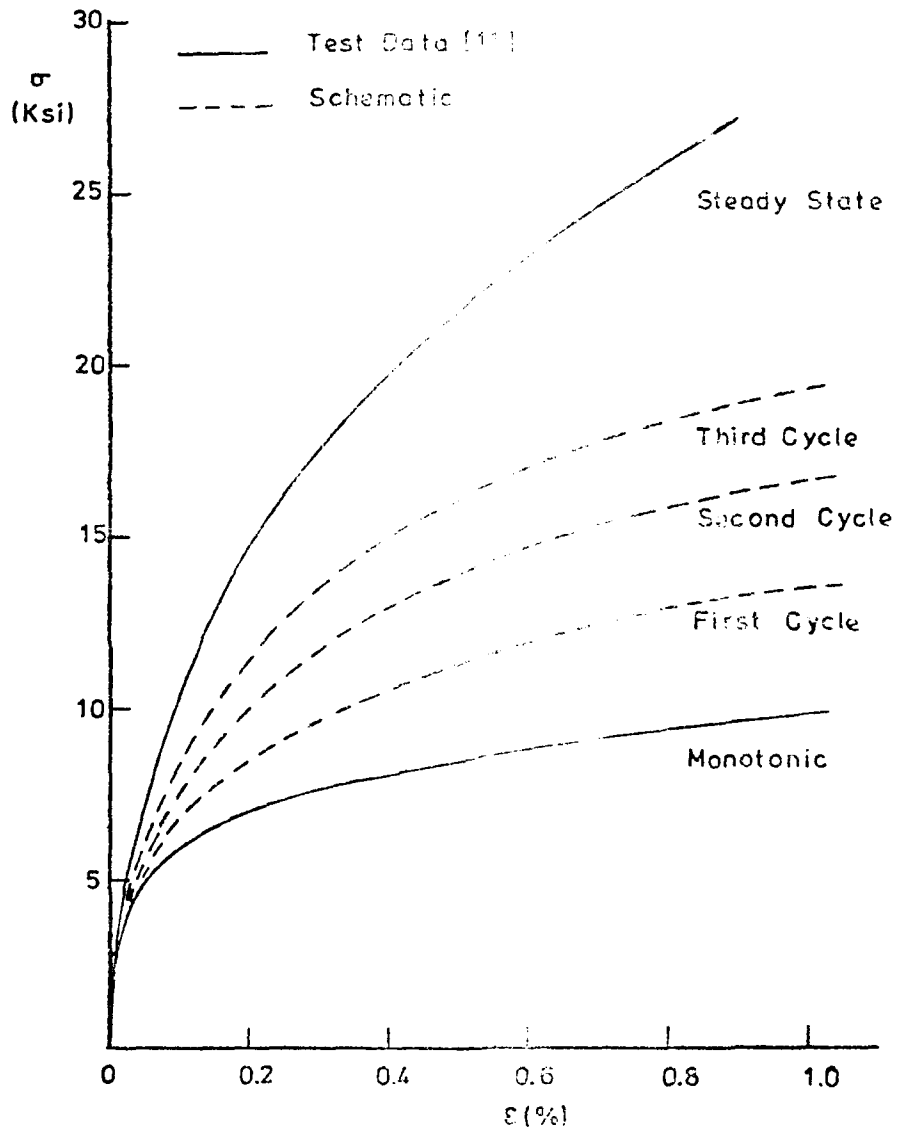


Fig. 1 Monotonic, *i*th Cycle and Steady State Cyclic Stress - Strain Curves for 99.9% Pure Copper [11].

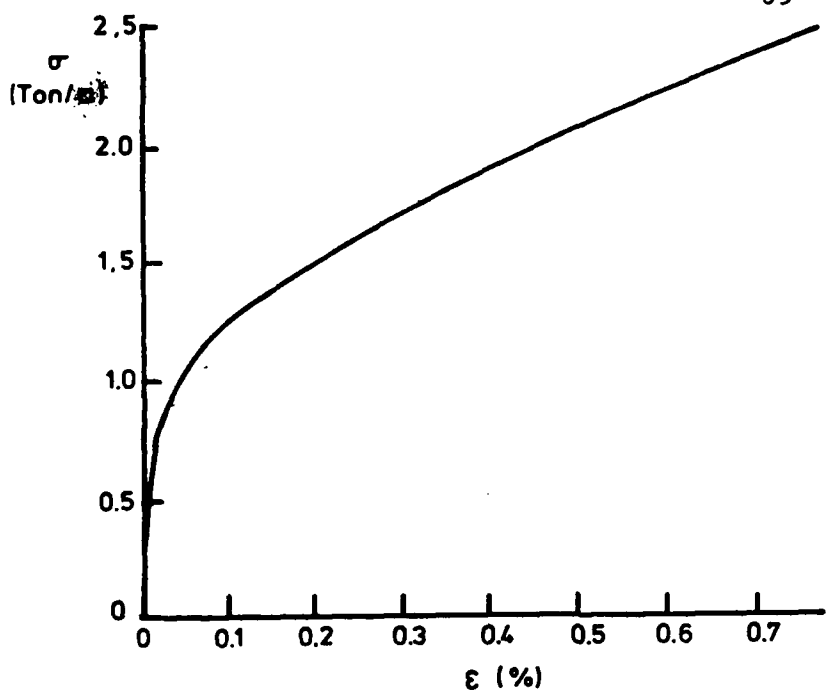


Fig.2a. Monotonic Stress-Strain Curve for Pure Copper[5]

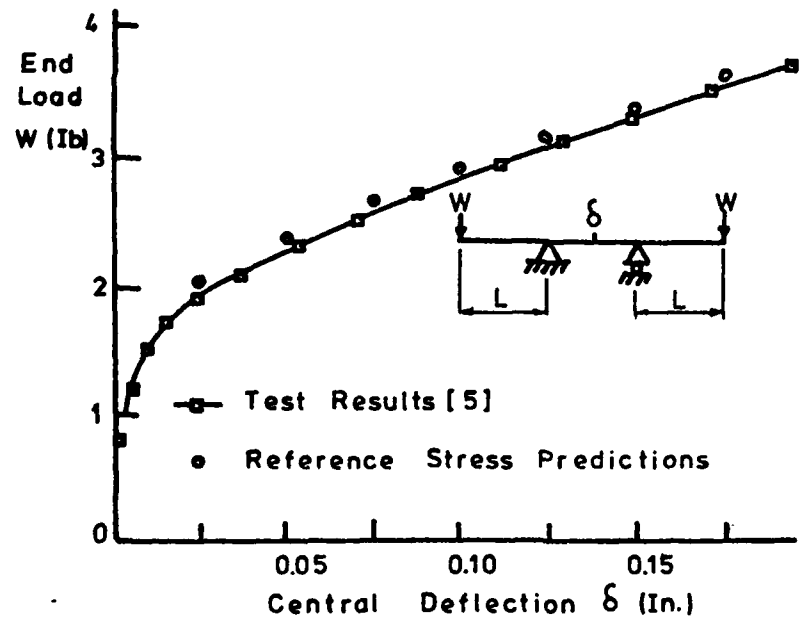


Fig.2b. Test Data and Reference Stress Predictions for a 4-Point Beam Bending Test on Pure Copper[5]

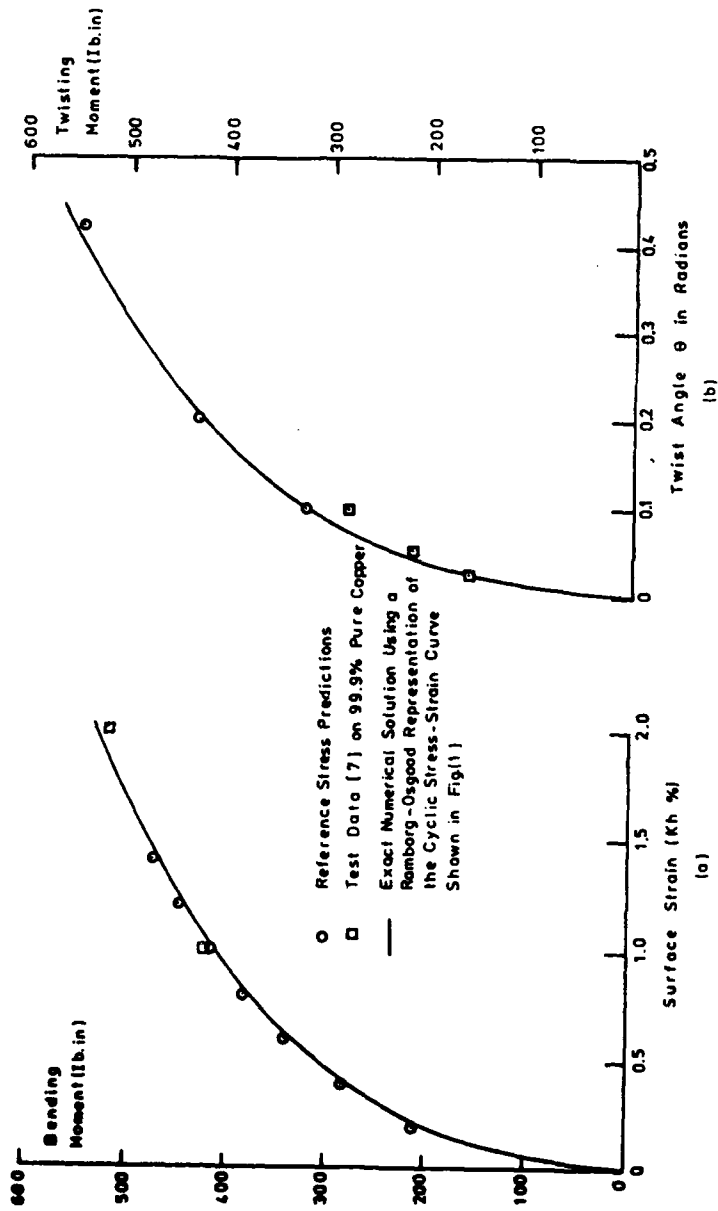


Fig.3 Cyclic Steady State Behaviour for a) Beam under Cyclic Curvature b) Solid Bar under Cyclic Twist.

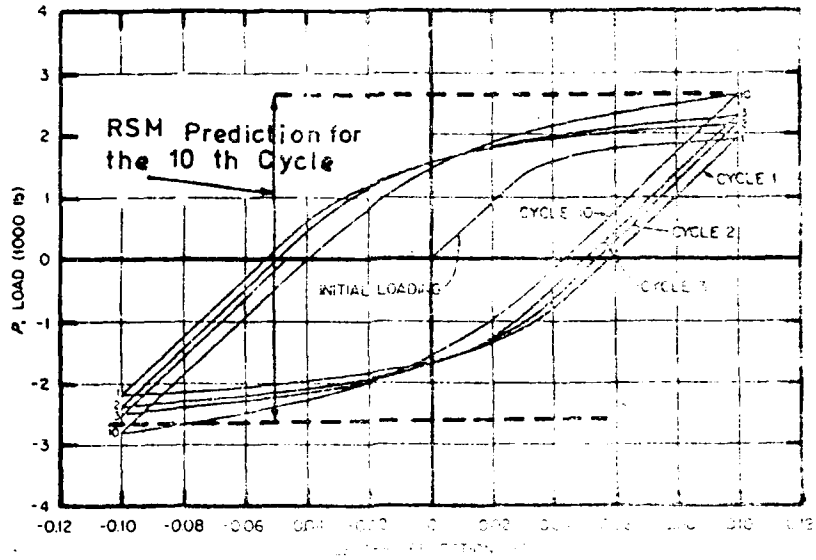


Fig. 4a. RSM Predictions of Test Results [8] of Simple Beam Under Cyclic Central Deflection.

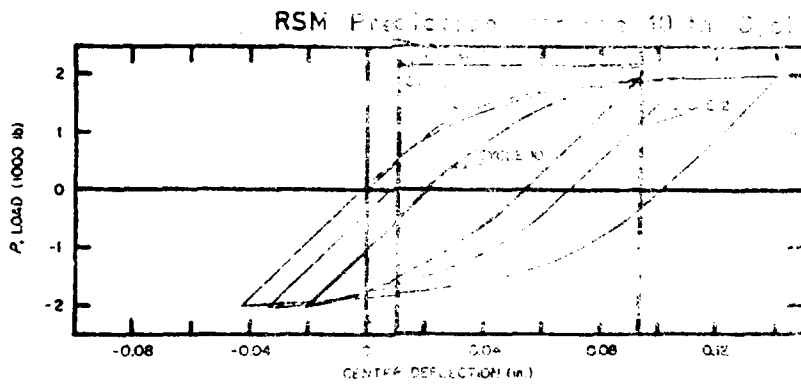


Fig. 4b. RSM Predictions of Test Results [11] of Simple Beam under Cyclic Central Load.

DATE
L MED
8